

REPORT DOCUMENTATION PAGE

Form Approved
OMB No. 0704-0188

The public reporting burden for this collection of information is estimated to average 1 hour per response, including the time for reviewing instructions, searching existing data sources, gathering and maintaining the data needed, and completing and reviewing the collection of information. Send comments regarding this burden estimate or any other aspect of this collection of information, including suggestions for reducing the burden, to the Department of Defense, Executive Service Directorate (0704-0188). Respondents should be aware that notwithstanding any other provision of law, no person shall be subject to any penalty for failing to comply with a collection of information if it does not display a currently valid OMB control number.

PLEASE DO NOT RETURN YOUR FORM TO THE ABOVE ORGANIZATION.

1. REPORT DATE (DD-MM-YYYY) 17-07-2014		2. REPORT TYPE Final Technical Report		3. DATES COVERED (From - To) From 15-07-2011 - To 14-07-2014	
4. TITLE AND SUBTITLE Innovative Advances in HPM: From Metamaterials to Buridan's Ass				5a. CONTRACT NUMBER	
				5b. GRANT NUMBER FA9550-11-1-0200	
				5c. PROGRAM ELEMENT NUMBER	
6. AUTHOR(S) Edl Schamiloglu and Sarita Project				5d. PROJECT NUMBER	
				5e. TASK NUMBER	
				5f. WORK UNIT NUMBER	
7. PERFORMING ORGANIZATION NAME(S) AND ADDRESS(ES) University of New Mexico Department of Electrical and Computer Engineering MSC01 1100 Albuquerque, NM 87131-0001				8. PERFORMING ORGANIZATION REPORT NUMBER 271362	
9. SPONSORING/MONITORING AGENCY NAME(S) AND ADDRESS(ES) AFOSR/RTB 875 N Randolph St. Arlington, VA 22203				10. SPONSOR/MONITOR'S ACRONYM(S) AFOSR	
				11. SPONSOR/MONITOR'S REPORT NUMBER(S)	
12. DISTRIBUTION/AVAILABILITY STATEMENT Distribution A: Approved for Public Release					
13. SUPPLEMENTARY NOTES					
14. ABSTRACT This report describes our research over the past three years to explore novel concepts in high power microwave (HPM) source physics. The metamaterials research proposed as part of this program focused on the use of a two-fold spiral corrugated Bragg reflector to both reflect the upstream propagating TM01 mode in an X-band backward-wave oscillator (BWO) and simultaneously convert it to a forward propagating Gaussian-like TE11 mode. We proposed to further explore a novel mode switching technique in a relativistic magnetron with diffraction output (MDO) driven by a transparent cathode. In earlier MAGIC simulations we had established that the qualitative picture of the dynamics of systems with two stable states separated by an unstable saddle point (hence, Buridan's Ass) is applicable to describe a new type of mode switching in an MDO. During the period of this grant our focus was redirected to support an EOARD-sponsored collaboration with a laboratory in Brazil. Finally, three supplemental funding actions took place on this grant. These are reported on as well.					
15. SUBJECT TERMS High Power Microwaves, HPM, Magnetron, Bragg Reflector, MILO					
16. SECURITY CLASSIFICATION OF:			17. LIMITATION OF ABSTRACT	18. NUMBER OF PAGES	19a. NAME OF RESPONSIBLE PERSON
a. REPORT	b. ABSTRACT	c. THIS PAGE			Edl Schamiloglu
Unlimited	Unlimited	Unlimited	Unlimited	47	19b. TELEPHONE NUMBER (Include area code) 505-277-4423



AFRL-OSR-VA-TR-2014-0172

Innovative Advances in HPM: From Metamaterials to Buridan's Ass

**Edl Schamiloglu
UNIVERSITY OF NEW MEXICO**

**07/23/2014
Final Report**

DISTRIBUTION A: Distribution approved for public release.

**Air Force Research Laboratory
AF Office Of Scientific Research (AFOSR)/ RTB
Arlington, Virginia 22203
Air Force Materiel Command**



THE UNIVERSITY of
NEW MEXICO SCHOOL of ENGINEERING

Department of Electrical & Computer Engineering

“Innovative Advances in HPM:
From Metamaterials to Buridan's Ass”

AFOSR Grant FA9550-11-1-0200

Final Technical Report
15 July 2011 – 14 July 2014

17 July 2014

Submitted by:

Edl Schamiloglu — Principal Investigator and Distinguished Professor
Department of Electrical and Computer Engineering
University of New Mexico
Albuquerque, NM 87131
Tel. (505) 277-4423
Fax: (505) 277-1439
e-mail: edls@unm.edu

TABLE OF CONTENTS

TABLE OF CONTENTS	2
LIST OF FIGURES	3
I. INTRODUCTION	4
II. TWO-FOLD SPIRAL CORRUGATED BRAGG REFLECTOR	5
III. RF MODE SWITCHING	11
IV. NLTL RESEARCH	17
V. RESEARCH FOR SUPPLEMENTAL FUNDING	18
A. MILO Testbed	18
B. Report for NSWC	20
VI. REFERENCES	21
VII. PERSONNEL, PUBLICATIONS, INTERACTIONS, AWARDS	22
PERSONNEL	22
PUBLICATIONS	22
RECOGNITION	26
NEW DISCOVERIES, INVENTIONS, PATENTS	26
APPENDIX A - FINAL REPORT FOR NSWC	27

LIST OF FIGURES

FIGURE 1. BACKWARD WAVE OSCILLATOR WITH A BRAGG REFLECTOR.	5
FIGURE 2. 2D VIEW OF THE TWO-FOLD SPIRAL CORRUGATED BRAGG REFLECTOR.	5
FIGURE 3. TWO LINEARLY POLARIZED PULSES FROM A SHORT PULSE RADAR.	5
FIGURE 4. DIMENSIONS OF THE BRAGG REFLECTOR.	6
FIGURE 5. MICROWAVE POWER AS A FUNCTION OF GUIDE MAGNETIC FIELD.	7
FIGURE 6. OUTPUT FREQUENCY AS A FUNCTION OF GUIDE MAGNETIC FIELD.	8
FIGURE 7. OUTPUT MICROWAVE PULSE.	9
FIGURE 8. OUTPUT FREQUENCY.	9
FIGURE 9. AZIMUTHAL COMPONENT OF THE ELECTRIC FIELD FOR THE TE_{11} MODE.	9
FIGURE 10. PHOTOGRAPH OF THE BRAGG REFLECTOR THAT IS READY FOR EXPERIMENTAL TESTING.	10
FIGURE 11. 12-CAVITY MDO DESIGN: (A) CROSS-SECTIONAL DIAGRAM IN THE R-Z PLANE (R IS THE RADIAL COORDINATE AND Z IS THE AXIAL ONE) AND ONE SUGGESTION OF IMPLEMENTING THE INJECTION OF AN INPUT SIGNAL USING A COAXIAL CABLE; (B) CROSS- SECTIONAL DIAGRAM IN THE R- θ PLANE (θ IS THE AZIMUTHAL COORDINATE); AND (C) 3-D VISUALIZATION OF THE 12-CAVITY MDO.	12
FIGURE 12. SEPARATION OF MODES WITH DIFFERENT AZIMUTHAL INDICES N BY THE APPLIED AXIAL MAGNETIC FIELD (FRAGMENTED FOR THE MOST POWERFUL HIGHER ORDER MODES). OUTPUT POWER P IN GW; RADIATION FREQUENCY F IN GHZ.	12
FIGURE 13. AXIAL DISTRIBUTIONS OF AZIMUTHAL ELECTRIC FIELD AT DIFFERENT FREQUENCIES OF THE TE_{41} - MODE: TOP - F = 2.7 GHZ; BOTTOM - F = 2.5 GHZ.	13
FIGURE 14. (LEFT) TWO STABLE STATES F_1 AND F_2 (LIMIT CIRCLES CORRESPONDING TO PERSISTENT OSCILLATIONS AND POINTS ARE FINAL STATES OF OSCILLATION WITH DAMPING) SEPARATED BY UNSTABLE SADDLE POINT F_0 . (RIGHT) BALL ON TOP OF A HILL BETWEEN TWO VALLEYS.	13
FIGURE 15. (LEFT) ELECTRON SPOKES SYNCHRONOUS WITH THE TE_{41} -MODE. (RIGHT) AZIMUTHAL FIELD STRUCTURE OF THE GENERATED TE_{41} -MODE.	14
FIGURE 16. (LEFT) OUTPUT POWER OF TE_{41} MODE GENERATION WHEN $H=4.8$ KOE. (RIGHT) SPECTRUM OF GENERATION WITH $f_1 = 2.5$ GHZ.	14
FIGURE 17. (LEFT) INPUT RF SIGNAL WITH FREQUENCY $f_2 = 2.7$. (MIDDLE) GENERATION OF THE SWITCHED TE_{41} MODE WITH FREQUENCY f_2 . (RIGHT) SPECTRUM OF SWITCHED MODE.	14
FIGURE 18. (LEFT) INPUT RF SIGNAL. (MIDDLE) RADIATION POWER OF THE TE_{41} MODE. (RIGHT) THE RADIATION SPECTRUM WHEN $H = 1.002H_{00}$ AND NOISE IS SUPPRESSED.	15
FIGURE 19. PHOTOGRAPHS OF THE MILO TESTBED.	18
FIGURE 20. CUT-AWAY VIEW OF THE MILO TESTBED.	19
FIGURE 21. MILO TESTBED IN THE LABORATORY.	19

I. INTRODUCTION

This final technical report describes our research over the past three years to explore novel concepts in HPM source physics. The title of the grant, “From Metamaterials to Buridan’s Ass,” reflects the breadth of the research that was proposed. The metamaterials research proposed as part of this program focused on the use of a two-fold spiral corrugated Bragg reflector to both reflect the upstream propagating TM_{01} mode in an X-band backward-wave oscillator (BWO) and simultaneously convert it to a forward propagating Gaussian-like TE_{11} mode. Buridan’s Ass refers to the famous dilemma posed by the need to make a decision between two equally attractive proposals. The concept itself dates from much earlier times, being discussed first by Aristotle (384-322 BC). In Buridan’s example, an ass faces starvation when it is unable to choose between two equally appetizing piles of hay. In the high power microwave (HPM) context, we proposed to further explore a novel mode switching technique in a relativistic magnetron with diffraction output (MDO) driven by a transparent cathode. In earlier MAGIC simulations we had established that the qualitative picture of the dynamics of systems with two stable states separated by an unstable saddle point (hence, Buridan’s Ass) is applicable to describe a new type of mode switching in an MDO.

During the period of this grant, Dr. José Osvaldo Rossi, Senior Researcher at National Institute for Space Research (INPE), Associated Plasma Laboratory (LAP), São José dos Campos, SP, Brazil, was awarded a series of EOARD grants to perform research on nonlinear transmission lines (NLTLs). Therefore, Prof. Schamiloglu redirected a small portion of this grant to collaborate with Dr. Rossi and Mr. Ngee Siang Kuek, a Ph.D. student that Prof. Schamiloglu was co-advising (Prof. Schamiloglu holds an appointment in the Department of Electrical and Computer Engineering, National University of Singapore).

Finally, supplemental funding was added to this grant on three occasions. The first was to support Dr. Salvador Portillo who contributed to the activities on this grant by developing a magnetically insulated line oscillator (MILO) test stand. The second was to support Prof. Schamiloglu for a paper study for the Naval Surface Warfare Center (NSWC). The third one was to support Dr. Thomas Hussey's participation in a high power RF working group for the Navy. The first two of these supplemental activities are included in this report. Dr. Hussey's work on the high power RF working group will be completed in the Fall 2014 and will be reported on separately.

II. TWO-FOLD SPIRAL CORRUGATED BRAGG REFLECTOR

A BWO is an O-type Cerenkov device that is designed to effectively convert electron beam kinetic energy into electromagnetic radiation. The output can be from S- to X-band microwave frequencies with powers over 100 MW. These devices are called O-type because the electrons travel along the axial guide magnetic field. The output mode pattern of the BWO is the TM_{01} mode where the distribution is a doughnut shape (*i.e.*, with a hole in the middle of the pattern). In order to provide for a more useful TE_{11} Gaussian-like output a two-fold spiral corrugated Bragg reflector has been used downstream of the cathode, as shown in Fig. 1.

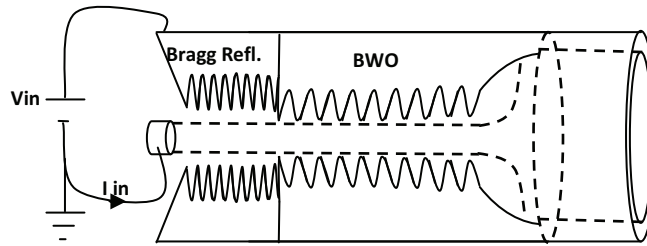


Figure 1. Backward wave oscillator with a Bragg reflector.

This Bragg reflector is a hollow circular waveguide with a two-fold spiral corrugated inner surface, as shown in Fig. 2. These counterwound spirals offer a linearly polarized output TE_{11} mode that is useful in short pulse radar applications, as an example. For instance, two orthogonal pulses shown in Fig. 3 can provide for a very detailed description of a target.



Figure 2. 2D view of the two-fold spiral corrugated Bragg reflector.

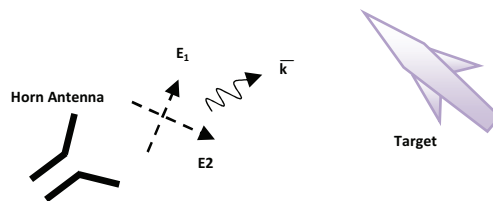


Figure 3. Two linearly polarized pulses from a short pulse radar.

Several methods were proposed to investigate metal waveguides with helical corrugations on the inner surface. A widely used approximate technique that was used in [1,2] is described as follows. The conversion process is between the TM_{01} and the TE_{11} modes at the same time that the Bragg reflector reflects back the electromagnetic wave generated in the BWO. A helical corrugation of the reflector with sinusoidal profile is shown in Fig. 4 and is describe by

$$R(\theta, z) = R_0 + l_0 \sin(hz \pm m\theta), \quad (1)$$

where $h = 2\pi/d$ is the periodic constant of the Bragg reflector; R , l_0 , and d are the average radius, amplitude of the spiral corrugation, and the axial period (along the axis), respectively. In addition, R_0 is the mean radius of the Bragg reflector, which is the average of the maximum and the minimum radii described by (2) and shown in Fig. 4.

$$R_0 = \frac{R_{max} + R_{min}}{2} \text{ and } l_0 = \frac{R_{max} - R_{min}}{2} \quad (2)$$

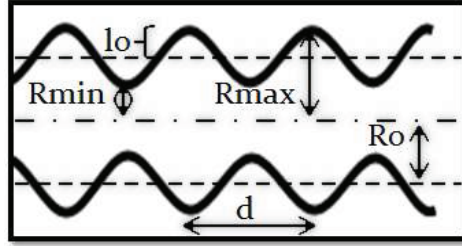


Figure 4. Dimensions of the Bragg reflector.

For effective reflection and conversion the corrugation depth should be less than the wavelength $l_0 \ll \lambda$ of the output wave. Furthermore, the plus and minus signs in (1) correspond to opposite directions of the spiral corrugations.

The number of spirals ($\pm m$) depends on the mode that the Bragg reflector will convert. In our case the conversion is between the TM_{01} and TE_{11} modes so that the number of spirals of the opposite direction corrugations can be obtained from (3)

$$m = \pm(m_H - m_E) = 1, \quad (3)$$

where $m_H = 1$ is the azimuthal index of the TM_{01} mode and $m_E = 0$ is the azimuthal index of the TE_{11} mode. The period of the Bragg reflector can be obtained from the periodic constant of the Bragg reflector h , which is the sum of the longitudinal wavenumbers of the TM_{01} and TE_{11} modes, given by

$$h_{TE_{11}} = \sqrt{k^2 - \left(\frac{p_{11}}{R_0}\right)^2} \text{ and } h_{TM_{01}} = \sqrt{k^2 - \left(\frac{p_{01}}{R_0}\right)^2}. \quad (4)$$

For a circular waveguide the Bessel function and its derivative roots are $p_{01} = 2.4048$ and $p_{11} = 1.8412$, respectively. In addition, the output frequency of interest is 10 GHz. Since the method of solving for the electromagnetic fields inside the Bragg reflector is approximate,

optimization of the dimensions is required. Table 1 summarizes the optimized parameters.

Table 1. Summary of the optimized parameters of the Bragg reflector.

Parameters	Symbols	Values
Inner radius	R_{\min}	0.700 inches
Outer radius	R_{\max}	0.899 inches
Mean radius	R_0	0.7995 inches
helical depth	ℓ_0	0.0995 inches
helical period	d	0.684 inches
Reflector length	L	8.208 inches
Fold number	m	1
Coupling Coefficient	$K_{E,H}$	0.94

When the inner radius of the Bragg reflector is chosen to be equal to the inner radius of the slow wave structure (SWS) of the BWO, two output frequencies were found. For the case that the electron beam propagates very close to the Bragg reflector inner wall the Bragg reflector section operates as an additional SWS.

The coupling coefficient between the TM_{01} and TE_{11} modes after the optimization was found to be 94% and can be calculated using (4) and (5) [1]

$$\delta = \frac{(\ell_0/2R_0)m_H k(h_{TE_{11}} + h_{TM_{01}})}{\sqrt{(h_{TE_{11}} * h_{TM_{01}}) * (p_{11}^2 - m_H^2)}}. \quad (5)$$

The length of the Bragg reflector is 8.208", which provides a conversion coefficient $K_p = K_{E,H}^2 \approx 0.88$, where $K_{E,H} = \tanh(\delta L)$.

The fully electromagnetic, fully relativistic particle-in-cell (PIC) code MAGIC [3] was used to study this Bragg reflector. First, a magnetic field scan was performed to find the optimal output power and range of frequency tuning, as show in Figs. 5 and 6.

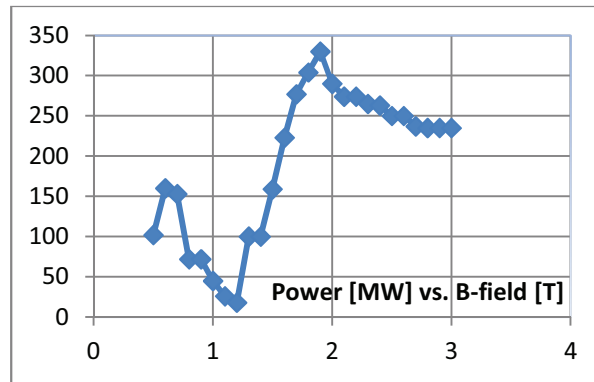


Figure 5. Microwave power as a function of guide magnetic field.

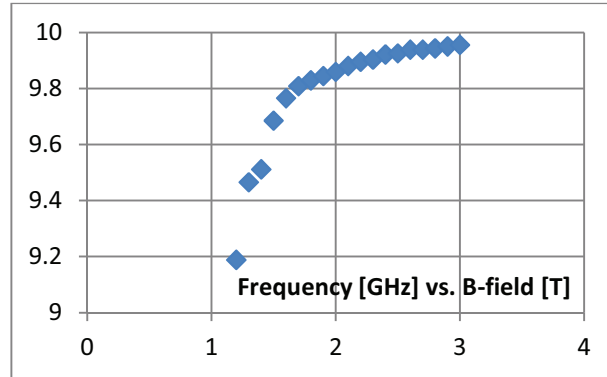


Figure 6. Output frequency as a function of guide magnetic field.

The BWO was driven using a voltage pulse that has a half sine wave-like shape with 460 kV-amplitude and 12 ns FWHM duration. The optimal guide magnetic field was 1.9 T. After using the the Bragg reflector's optimal dimensions (Table 1) and optimized electron beam parameters (Table 2) a narrow Gaussian-like wave beam with a power of more than 330 MW at 9.9 GHz was observed, as shown in Figs. 7 and 8.

Table 2. Summary of the electron beam and magnetic field parameters used to drive the BWO.

Parameters	Values
Beam voltage	460 kV
Beam current	4.3 kA
Magnetic field	1.9 T
Microwave power	330 MW
Operating frequency	10 GHz
Efficiency	16.5%
Electrical Tuning	800 MHz

From our earlier work [4] we know that the mode that was generated in the BWO is the TM_{01} mode. In Fig. 9 we observe that the reflected wave is successfully converted to the TE_{11} mode.

Construction of the Bragg reflector has been completed, as shown in Fig. 10 (it took three months to machine it!), and experimental testing will commence in the Fall 2014.

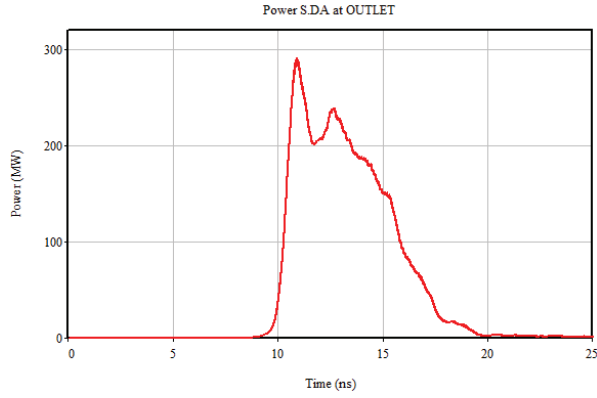


Figure 7. Output microwave pulse.

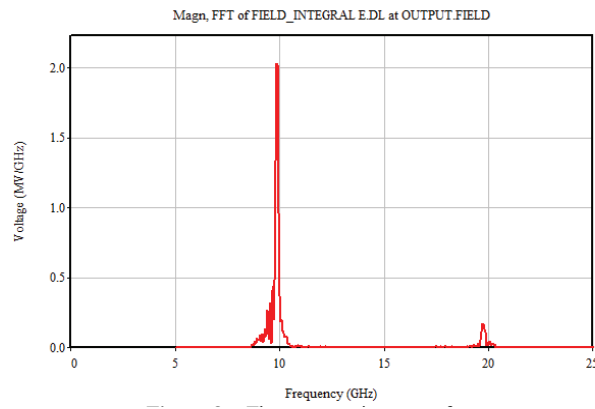


Figure 8. Output frequency.

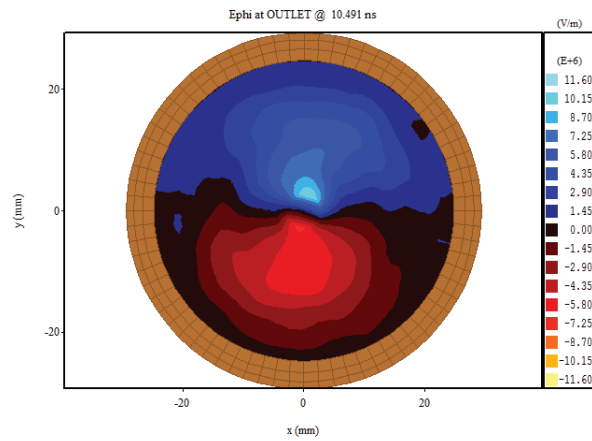


Figure 9. Azimuthal component of the electric field for the TE_{11} mode.

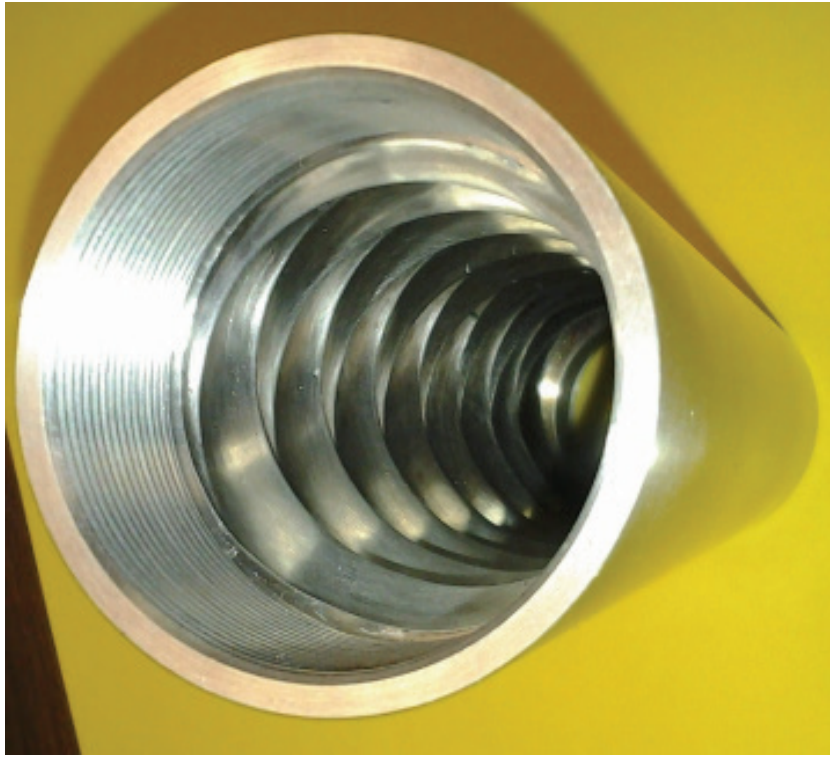


Figure 10. Photograph of the Bragg reflector that is ready for experimental testing.

III. RF MODE SWITCHING

The possibility of mode switching from one pulse to another in a 6-cavity gigawatt MDO using a weak (200–300 kW), short (15-ns), and single-frequency RF signal was demonstrated using particle-in-cell simulations in our earlier work [5]. This mode switching exploits the symmetric nature of the MDO that facilitates the use of any eigenmode as the operating mode. All scenarios of mode switching were considered using common properties of dynamical systems with two stable states separated by an unstable saddle point. In this portion of the grant research we continued to study the problem of mode switching, but this time for a 12-cavity MDO, for which we found splitting of the radiation frequency for each eigenmode owing to its different longitudinal distributions. Since splitting manifests as a bifurcation of frequency for definite values of the applied axial magnetic field, scenarios of frequency switching for this 12-cavity magnetron are considered.

MDOs are magnetrons with axial extraction of radiation through a horn antenna in which cavities of an anode block are continued along the antenna wall up to a cross section that exceeds the cutoff section for a radiated wave [6]. In an MDO, any mode can be used as the operating mode owing to its symmetric nature [7]. This is unlike the case with magnetrons having asymmetric output structures (for example, extracting radiation through one of the cavities of the anode block), in which only nondegenerate modes can be used for operation [8] and hopping to other modes can lead to excitation of an unloaded mode, resulting in overheating and erosion of magnetron electrodes. To avoid such a dangerous situation, different means are applied to provide stable generation with, as a rule, the operating π -mode (straps or anode block with rising sun cavities [8]).

Among many possible versions of an MDO, we identified an interesting one that possesses the necessary requirements for demonstrating frequency splitting attributed to modes having identical transverse field structure but different longitudinal distributions. This MDO (see Fig. 11) has the same dimensions as the A6 MDO [9], but the number of 20° sectorial cavities is increased from 6 to 12, decreasing the distance between them from 40° to 10° . Unlike [5] in which the 6-cavity MDO was optimized in order to achieve the maximal electronic efficiency $\eta_e = P/UI_a$ and the maximal radiation power P for the neighboring π -mode and $4\pi/3$ -mode (that is the negative first spatial harmonic of the $2\pi/3$ -mode) with good matching to the load, for the 12-cavity design, we have not optimized the dimensions. Here, I_a is the anode current. Nevertheless, our PIC simulations of the 12-cavity MDO for an applied voltage $U = 400$ kV and voltage rise time of 4 ns show (see Fig. 12) that output power and efficiency for some eigenmodes (not for the π -mode) are high (for the TE_{31} -mode, $P \approx 1.3$ GW and $\eta_e \approx 50\%$; for the TE_{41} -mode, $P \approx 1.5$ GW and $\eta_e \approx 63.5\%$). The total efficiency $\eta = P/UI$ is not shown because total current $I = I_a + I_{\text{end}}$ can be close to I_a since there are many different means to decrease the end-loss current I_{end} in magnetrons that consists of electron flows from the interaction space and the cathode edge. In simulations using the PIC code MAGIC we use a transparent cathode consisting of 12 separate longitudinal emitters periodically placed about radius $R_c = 10$ mm. It can be inferred that, for modes with azimuthal indices $n = 3$ and 4, reflection coefficients R_{ref} are maximal; therefore, the loaded Q-factor, which is close to the diffraction Q-factor

$$Q \approx Q_{\text{dif}} = \frac{8\pi (L/\lambda)^2}{m(1-R_{\text{ref}})} \quad (6)$$

is high, and as a consequence, the microwave electric field is strongest. Here, m is the number of axial field variations, L is the length of the interaction space, and λ is the wavelength. Figure 12 indicates that there is not only a good separation of eigenmodes TE_{n1} depending on the applied axial magnetic field H , but also that frequency splitting for any eigenmode occurs, which corresponds to different axial microwave field distributions (see Fig. 13). Thus, for this MDO, there are definite values of the applied magnetic field corresponding to frequency bifurcation between regions of synchronous interaction of electrons with neighboring transverse modes and frequency bifurcation within each region between modes with different axial distributions but with the same transverse field structure.

Both types of modes, those with different transverse structures as well as with different axial structures, generate their own frequencies; therefore, the coupling of each mode with the cathode electron flow is different as well. As a consequence, the power radiated for each mode is different and the dependence of this power on the applied magnetic field (see Fig. 12) can have explicit, as well as hidden interruptions.

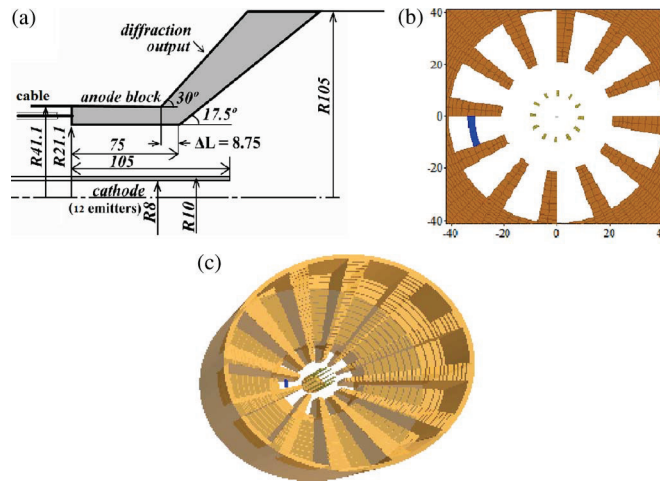


Figure 11. 12-cavity MDO design: (a) Cross-sectional diagram in the r - z plane (r is the radial coordinate and z is the axial one) and one suggestion of implementing the injection of an input signal using a coaxial cable; (b) cross-sectional diagram in the r - θ plane (θ is the azimuthal coordinate); and (c) 3-D visualization of the 12-cavity MDO.

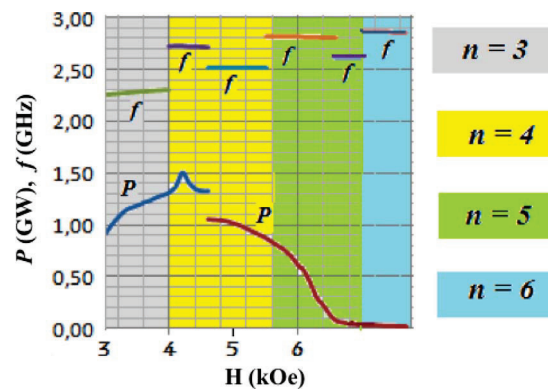


Figure 12. Separation of modes with different azimuthal indices n by the applied axial magnetic field (fragmented for the most powerful higher order modes). Output power P in GW; radiation frequency f in GHz.

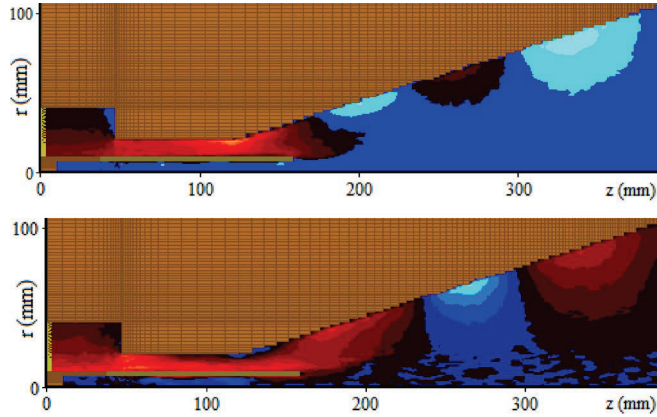


Figure 13. Axial distributions of azimuthal electric field at different frequencies of the TE_{41} -mode: top – $f = 2.7$ GHz; bottom – $f = 2.5$ GHz.

The bifurcation of frequency gives the possibility to consider switching of frequencies related to the same transverse eigenmode using common properties of a dynamical system with two stable states separated by an unstable saddle point. Following [10], such a situation is presented in a phase plane [see Fig. 14 (left)], where limit circles correspond to persistent oscillations with permanent amplitude and particular points in the centers of the limit circles are final states of oscillations when damping is present. As in [5], it is convenient to consider all scenarios of frequency switching using the mechanical analog of the aforesaid dynamical system, *i.e.*, a ball on top of a hill between two valleys [see Fig. 14 (right)].

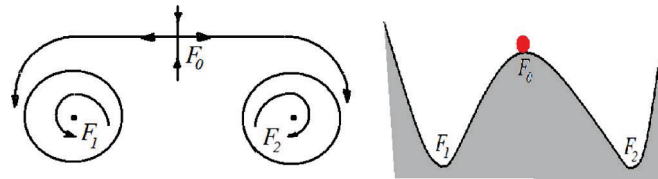


Figure 14. (Left) Two stable states F_1 and F_2 (limit circles corresponding to persistent oscillations and points are final states of oscillation with damping) separated by unstable saddle point F_0 . (Right) Ball on top of a hill between two valleys.

Let us consider the problem of frequency switching for the 400 kV 12-cavity MDO operating in the TE_{41} -mode (see Fig. 12) for which the critical magnetic field $H_{00} \approx 4.7$ kOe (*i.e.*, the field where bifurcation of frequencies $f_1 \approx 2.5$ GHz and $f_2 \approx 2.7$ GHz occurs).

The position of the ball on top of the hill is unstable. It is impossible to predict the direction that the ball will be rolling due to microscopic perturbations. Similarly, for the MDO, when $H = H_{00}$ it is impossible to predict which frequency the MDO will oscillate in. In order to avoid such uncertainty, let us slightly shift the initial position of the ball, for example, to the left. Then, the ball deterministically rolls to valley F_1 . A similar situation occurs when we choose a value of the magnetic field in the MDO that is slightly greater than the critical value H_{00} , for example, $H = 4.8$ kOe. Then, the TE_{41} -wave will deterministically oscillate with frequency $f_1 \approx 2.5$ GHz (see Figs. 15 and 16).

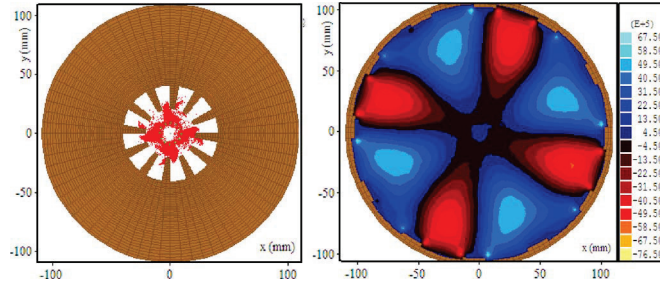


Figure 15. (Left) Electron spokes synchronous with the TE₄₁-mode. (Right) Azimuthal field structure of the generated TE₄₁-mode.

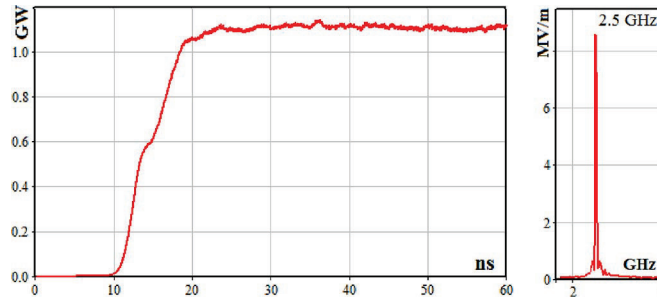


Figure 16. (Left) Output power of TE₄₁ mode generation when H=4.8 KOe. (Right) Spectrum of generation with $f_1 = 2.5$ GHz.

If one were to nudge the ball to the right from the chosen new initial position, the ball will roll to valley F_2 . In so doing, the closer the ball's initial position is to the top, the weaker is the impulse that is required for the ball to roll to the right. Similarly, the closer the magnetic field in the MDO is to the critical value, the weaker is the RF signal with frequency f_2 that is needed in order to generate this new frequency (see Fig. 17).

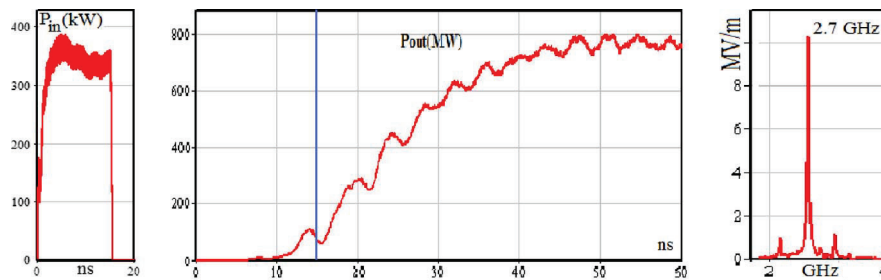


Figure 17. (Left) Input RF signal with frequency $f_2 = 2.7$. (Middle) Generation of the switched TE₄₁ mode with frequency f_2 . (Right) Spectrum of switched mode.

We apply a short-pulse (15 ns) and weak (350 kW) input RF signal (2.7 GHz) that switches the oscillation frequency, and the generation of the switched frequency persists in spite of removing the input signal [this moment is shown by the blue line in the dependence $P_{\text{out}}(t)$ in Fig. 17 (middle)]. The modulation in the amplitude is caused by the presence of a small amount of the original frequency due to the proximity to the boundary H_{00} between these two regions.

One would think that we should be able to select a magnetic field that is arbitrarily close to H_{00} such that any small input signal can switch frequencies. This is incorrect because the inevitable presence of noise leads to the erosion of the boundary between the two regions such that it is impossible to choose H arbitrarily close to H_{00} because the number of shots with unpredictable oscillation frequency increases very rapidly. We have checked this for $H = 1.002H_{00}$ in MAGIC simulations (the option “MAXWELL HIGH Q” allows for different levels of damping of the numerical noise). With strong noise damping, we found the situation, when frequency switching is achieved using a very weak input signal, less than 10 kW [see Fig. 18 (left)]. Even with numerical noise damping, beats are observed as amplitude modulation [see Fig. 18 (middle)] caused by the presence of another frequency $f_1 \approx 2.5$ GHz [see Fig. 18 (right)] because of the proximity to the critical magnetic field H_{00} , and competition between axial field structures corresponding to these frequencies becomes more violent with increased noise level.

In [11], the initial energy of electron noise was estimated to be 10 orders of magnitude lower than the energy of the electron hub drifting around the cathode in crossed applied electric and magnetic fields; however, while the threshold of generation is not exceeded, a magnetron is a regenerative amplifier of noise; therefore, the longer the rise time of the applied voltage, the higher the level of amplifying noise. Since it is impossible to compare numerical noise with real noise, in planned experiments, we will check what weak signal can be used for frequency switching in the 12-cavity MDO. In our studies thus far, when the difference $|H - H_{00}|/H_{00} \geq 2\%$, which we used in computer simulations with standard (85%) suppression of noise in MAGIC, unpredictable situations have yet to be encountered.

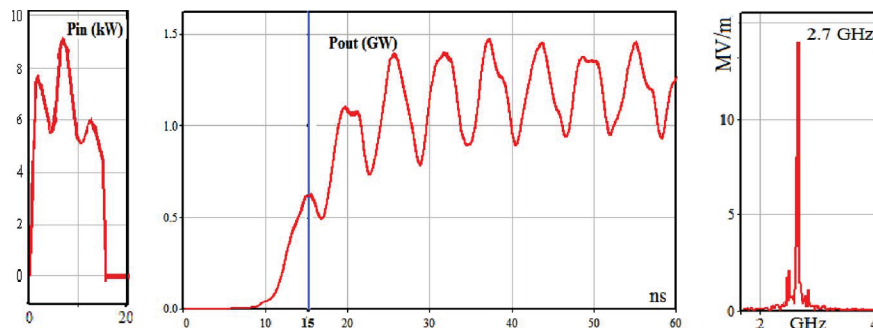


Figure 18. (Left) Input RF signal. (Middle) Radiation power of the TE_{41} mode. (Right) The radiation spectrum when $H = 1.002H_{00}$ and noise is suppressed.

We have demonstrated frequency switching in an MDO not only by switching neighboring eigenmodes with different azimuthal indices but also by switching neighboring longitudinal modes with the same transverse field structure. The closer the applied magnetic field is to the critical value, the weaker is the required input signal to switch the modes. Approaching the critical value is limited by inevitable noise that erodes the boundary between regions of generation of adjacent modes that manifest in very rapidly increasing the number of shots with unpredictable oscillation frequency. Another consequence of operating at magnetic fields near the critical value is that the output power

envelope shows larger oscillations. For magnetic fields farther from the critical value the output power envelope shows smaller oscillations, and the spectrum is cleaner in this case as well. In our simulations, we observe that the field interaction is strongest when the magnetron operates in the TE_{41} -mode and its output power is greatest. As in our earlier work [5], we demonstrate that a short input signal of order 100-kW can be used to switch gigawatt output power with different operating frequencies.

IV. NLTL RESEARCH

Professor Schamiloglu and his group have been collaborating with Dr. José Osvaldo Rossi, Senior Researcher at National Institute for Space Research (INPE), Associated Plasma Laboratory (LAP), São José dos Campos, SP, Brazil. Dr. Rossi was awarded a series of EOARD grants to perform research on nonlinear transmission lines (NLTLs). Therefore, Prof. Schamiloglu redirected a small portion of this grant to collaborate with Dr. Rossi and Mr. Ngee Siang Kuek, a Ph.D. student that Prof. Schamiloglu was co-advising (Prof. Schamiloglu holds an appointment in the Department of Electrical and Computer Engineering, National University of Singapore).

A nonlinear lumped element transmission line (NLETL) that consists of a LC ladder network can be used to convert a rectangular input pump pulse to a series of RF oscillations at the output. The discreteness of the LC sections in the network contributes to the line dispersion while the nonlinearity of the LC elements produces the nonlinear characteristics of the line. Both of these properties combine to produce wave trains of high frequency. Three types of lines were studied in this collaboration: a) nonlinear capacitive line (NLCL) where only the capacitive component is nonlinear; b) nonlinear inductive line (NLIL) where only the inductive component is nonlinear; and c) nonlinear hybrid line (NLHL) where both LC components are nonlinear. Based on circuit theory, a NLETL circuit model was developed for simulation and extensive parametric studies were carried out to understand the behavior and characteristics of these lines. Generally, results from the NLETL model showed good agreement to the experimental data. The voltage modulation and the frequency content of the output RF pulses were analyzed. An innovative method for more efficient RF extraction was implemented in the NLCL. A simple novel method was also found to obtain the necessary material parameters for modeling the NLIL. For better matching to resistive load, the NLHL (where no experimental NLHL has been reported to date) was successfully demonstrated in experiment.

This fruitful collaboration resulted in four journal articles:

1. N.S. Kuek, A.C. Liew, E. Schamiloglu, and J.O. Rossi, "Circuit Modeling of Nonlinear Lumped Element Transmission Lines including Hybrid Lines," *IEEE Trans. Plasma Sci.*, vol. 40, 2523-2534 (2012).
2. N.S. Kuek, A.C. Liew, E. Schamiloglu, and J.O. Rossi, "Pulsed RF Oscillations on a Nonlinear Capacitive Transmission Line," *IEEE Trans. Dielectrics and Elect. Insul.*, vol. 20, 1129-1135 (2013).
3. N.S. Kuek, A.C. Liew, E. Schamiloglu, and J.O. Rossi, "Oscillating Pulse Generator Based on a Nonlinear Inductive Line," *IEEE Trans. Plasma Sci.*, vol. 41, 2619-2624 (2013).
4. N.S. Kuek, A.C. Liew, E. Schamiloglu, and J.O. Rossi, "Pulse Generator Based on a Nonlinear Hybrid Line," accepted and to appear in *IEEE Trans. Plasma Sci.* (2014).

V. RESEARCH FOR SUPPLEMENTAL FUNDING

A. MILO Testbed

Supplemental funding was provided for a 12-month effort to support Dr. Salvador Portillo and his effort to construct a MILO testbed. This testbed is intended to provide diagnostic access in order to perform plasma measurements to compare with recent LSP simulations describing the effects of electrode plasmas on MILO performance [12].

Radiation pulse shortening in long pulsed beam driven sources, low efficiency, as well as poor repetition rate has long posed a problem for HPM sources and limited their use for DOD applications. A MILO testbed has been designed and constructed in order to:

1. To investigate the plasma closure mechanism leading to pulse shortening in magnetically insulated HPM devices such as Magnetrans and MILOs. Models point to low density plasmas evolving from the cathode surface as the main driver of radiation collapse.
2. Develop materials and techniques to mitigate this plasma closure and increase the pulse length in excess of 500 ns. Carbon nanotube cathodes, transparent cathodes, carbon fiber cathodes will be considered.
3. Understand and solve the ion production and gap closure problem to yield solutions for repetitive pulsing of beam driven HPM sources.
4. Develop a more thorough understanding of the beam physics in magnetically insulated devices to increase the energy transfer efficiency.
5. Compare with LSP simulations.

Figures 19-21 present details of the constructed MILO testbed.

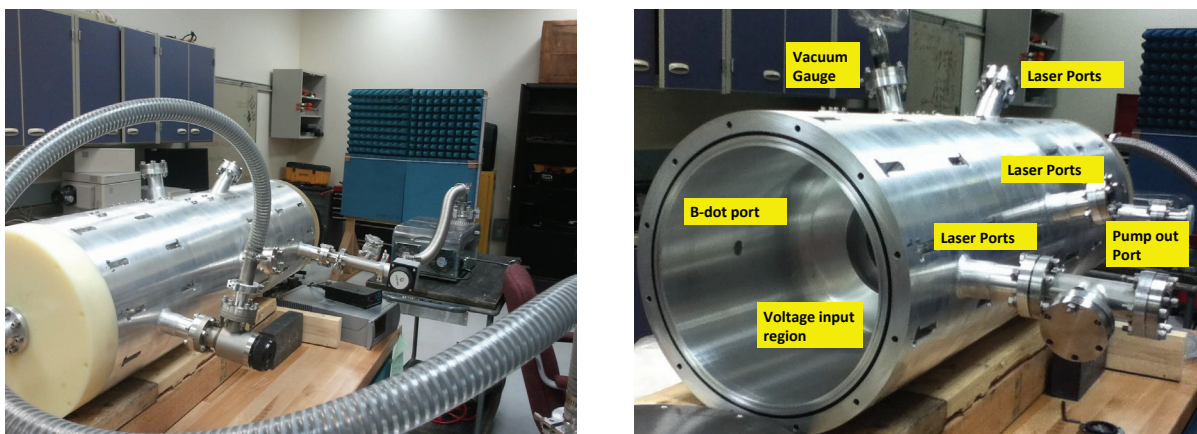


Figure 19. Photographs of the MILO testbed.

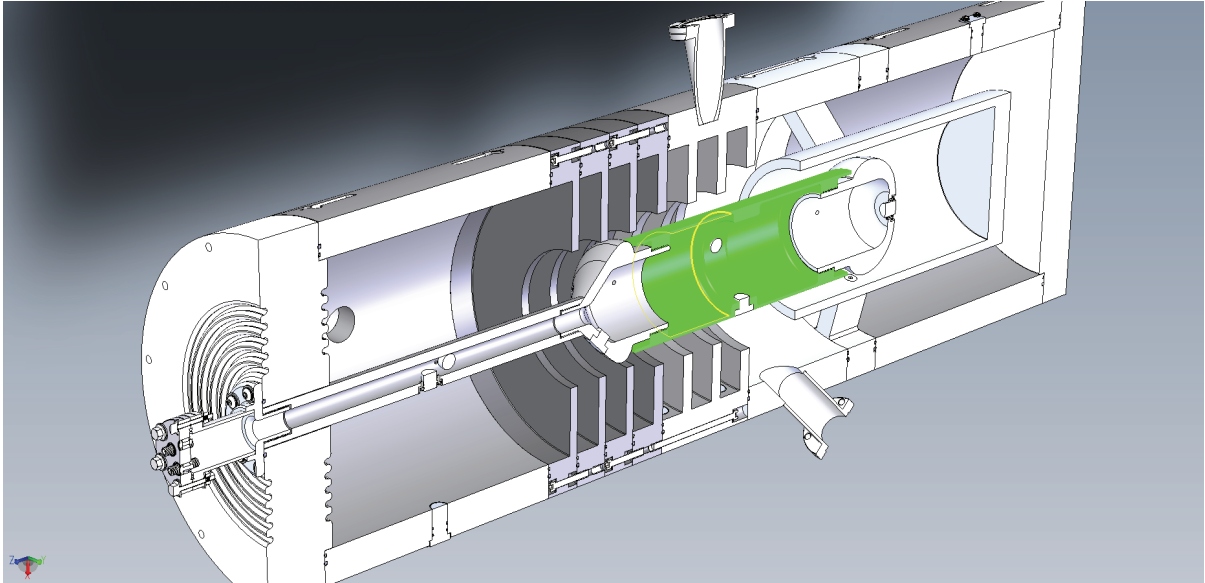


Figure 20. Cut-away view of the MILO testbed.

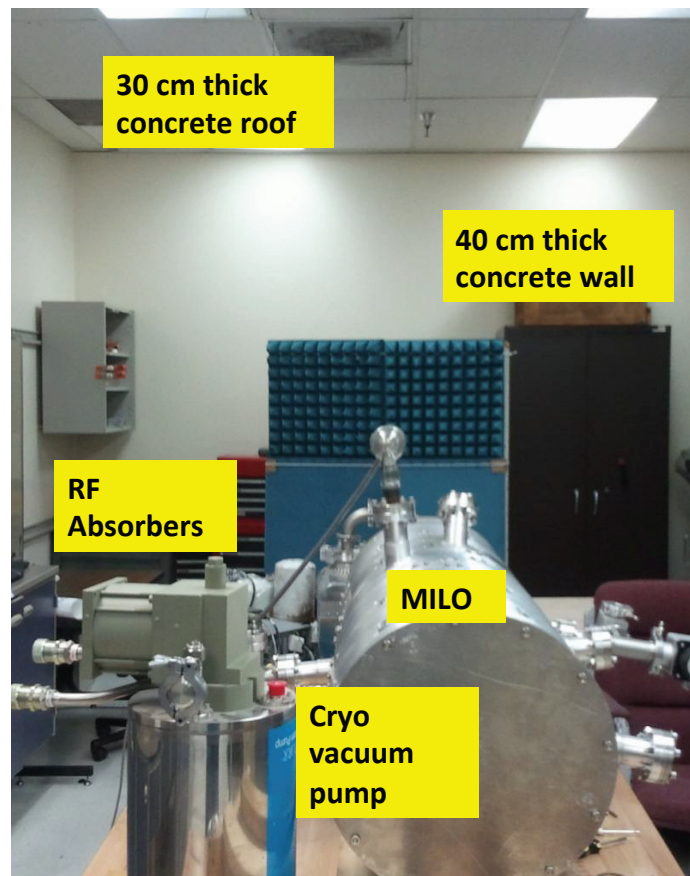


Figure 21. MILO testbed in the laboratory.

B. Report for NSW

Professor Schamiloglu was tasked to perform an HPM Technology Evaluation for NSW. This was a three-month effort and the final report is attached as Appendix A to this report.

VI. REFERENCES

- [1] M.I. Fuks, V.A. Gintsburg, N.G. Kolganov, and E. Schamiloglu, "Experimental Study of a Relativistic Resonant Traveling-Wave Tube with Selective Feedback Provided by Bragg Reflectors," *IEEE Trans. Plasma Sci.*, vol. 38, pp. 1255-1263 (2010).
- [2] M.I. Fuks, M.B. Goikhman, N.F. Kovalev, A.V. Palitsin, and E. Schamiloglu, "Waveguide Resonators with Combined Bragg Reflectors," *IEEE Trans. Plasma Sci.*, vol. 32, pp. 1323-1333 (2004).
- [3] B. Goplen, L. Ludeking, D. Smith, and G. Warren, "User-Configurable MAGIC for Electromagnetic PIC Calculations," *Comput. Phys. Commun.*, vol. 87, pp. 54–86 (1995).
- [4] S. Prasad, C.J. Buchenauer, M. Fuks, C. Leach, M. Roybal, and E. Schamiloglu, "X-band Relativistic BWO with Frequency Tuning," *IEEE International Conference on Plasma Science* (San Diego, CA, June 1-5, 2009).
- [5] M. Liu, C. Michel, S. Prasad, M. Fuks, E. Schamiloglu, and C.-L. Liu, "RF Mode Switching in a Relativistic Magnetron with Diffraction Output," *Appl. Phys. Lett.*, vol. 97, pp. 251 501–251 503 (2010).
- [6] N.F. Kovalev, B.D. Kol'chugin, V.E. Nechaev, M.M. Ofitserov, E.I. Soluyanov, and M.I. Fuks, "Relativistic Magnetrons with Diffraction Output of Electromagnetic Radiation," *Sov. Tech. Phys. Lett.*, vol. 3, pp. 430–433 (1977).
- [7] M.I. Fuks and N.F. Kovalev, "Relativistic Magnetron with Diffraction Output," in *Proc. Progr. Abst. XI Int. Conf. High-Power Electromagn.* (Tel Aviv, Israel, 1998), p. 18.
- [8] G.B. Collins, Ed., *Microwave Magnetrons* (McGraw-Hill, New York, NY, 1948).
- [9] M. Fuks and E. Schamiloglu, "70% Efficient Relativistic Magnetron with Axial Extraction of Radiation through a Horn Antenna," *IEEE Trans. Plasma Sci.*, vol. 38, pp. 1302–1312 (2010).
- [10] A.A. Andronov, A.A. Witt, and S.E. Khaikin, *Theory of Oscillations* (Pergamon Press, Oxford, U.K., 1966).
- [11] O. Buneman, "Symmetric States and their Disruption," in *Crossed-Field Microwave Devices*, E. Okress, Ed. (Academic Press, New York, NY, 1961), pp. 181–203.
- [12] D.V. Rose, C.L. Miller, S. Portillo, and D.R. Welch, "Electrode-Plasma-Driven Radiation Cutoff in Long-Pulse, High-Power Microwave Devices," *Phys. Plasmas*, vol. 20, 034501-01-04 (2013).

VII. PERSONNEL, PUBLICATIONS, INTERACTIONS, AWARDS

PERSONNEL

Dr. Edl Schamiloglu	Professor and PI
Dr. Mikhail Fuks	Research Professor
Dr. Sarita Prasad	Research Assistant Professor
Mr. Ahmed Elfrgani	Ph.D. student
Dr. Salvador Portillo	Research Associate Professor

PUBLICATIONS

A. Journal Papers

1. C. Watts, M. Gilmore, and E. Schamiloglu, "Effects of Laser Surface Modification on Secondary Electron Emission of Copper," *IEEE Trans. Plasma Sci.*, vol. 39, 836-841 (2011).
2. M. Liu, C.-L. Liu, D. Galbreath, C. Michel, S. Prasad, M.I. Fuks, and E. Schamiloglu, "Frequency Switching in a Relativistic Magnetron with Diffraction Output," *J. Appl. Phys.*, vol. 110, 033304-1-7 (2011).
3. M. Liu, M. Fuks, E. Schamiloglu, and C.-L. Liu, "Frequency Switching in a 12-Cavity Relativistic Magnetron with Axial Extraction of Radiation," *IEEE Trans. Plasma Sci.*, vol. 40, 1569-1574 (2012).
4. N.S. Kuek, A.C. Liew, E. Schamiloglu, and J.O. Rossi, "Circuit Modeling of Nonlinear Lumped Element Transmission Lines including Hybrid Lines," *IEEE Trans. Plasma Sci.*, vol. 40, 2523-2534 (2012).
5. S. Soh, R.B. Miller, E. Schamiloglu, and C. G. Christodoulou, "Dual Mode Reltron," *IEEE Trans. Plasma Sci.*, vol. 40, 2083-2088 (2012).
6. N.S. Kuek, A.C. Liew, E. Schamiloglu, and J.O. Rossi, "Pulsed RF Oscillations on a Nonlinear Capacitive Transmission Line," *IEEE Trans. Dielectrics and Elect. Insul.*, vol. 20, 1129-1135 (2013).
7. N.S. Kuek, A.C. Liew, E. Schamiloglu, and J.O. Rossi, "Oscillating Pulse Generator Based on a Nonlinear Inductive Line," *IEEE Trans. Plasma Sci.*, vol. 41, 2619-2624 (2013).
8. K.J. Hendricks, A.D. Andreev, S. Soh, M.I. Fuks, and E. Schamiloglu, "Elemental Theory of a Relativistic Magnetron Operation: Dispersion Diagram," *J. Directed Energy*, vol. 5, 1-41 (2013).
9. N.S. Kuek, A.C. Liew, E. Schamiloglu, and J.O. Rossi, "Pulse Generator Based on a Nonlinear Hybrid Line," accepted and to appear in *IEEE Trans. Plasma Sci.* (2014).
10. H. Canacsinh, L.M. Redondo, J. Fernando Silva, and E. Schamiloglu, "Solid-State Bipolar Marx Modulator Modeling," accepted and to appear in *IEEE Trans. Plasma Sci.* (2014).

B. Papers in Conference Proceedings

1. N.S. Kuek, A.C. Liew, E. Schamiloglu, and J. Rossi, "Circuit Modeling of Nonlinear Lumped Element Transmission Lines," *Proc. 18th IEEE International Pulsed Power Conference* (Chicago, IL, 2011), p. 185-192.

2. N.S. Kuek, A.C. Liew, and E. Schamiloglu, "Experimental Demonstration of Nonlinear Lumped Element Transmission Lines Using COTS Components," *Proc. 18th IEEE International Pulsed Power Conference* (Chicago, IL, 2011), p. 193-198.
3. M. Liu, M.I. Fuks, E. Schamiloglu, and C.-L. Liu, "RF Input for Sectioned Relativistic Amplifiers," *Proc. 18th IEEE International Pulsed Power Conference* (Chicago, IL, 2011), p. 367-370.
4. S. Soh, E. Schamiloglu, and R.B. Miller, "Design of a Dual Cavity Reltron," *Proc. 18th IEEE International Pulsed Power Conference* (Chicago, IL, 2011). p. 653-657.
5. C.L. Mendonca, T. Fleming, S. Prasad, and E. Schamiloglu, "3D ICEPIC Simulations of A6 Magnetron with Transparent Cathode for Comparison of 3D MAGIC Simulations," *Proc. 18th IEEE International Pulsed Power Conference* (Chicago, IL, 2011), p. 823-828.
6. M. Liu, M.I. Fuks, E. Schamiloglu, and C.-L. Liu, "RF Frequency Switching in a Relativistic Magnetron with Diffraction Output (MDO)," *Proc. 18th IEEE International Pulsed Power Conference* (Chicago, IL, 2011), p. 829-832.
7. H. Canacsinh, L.M. Redondo, F.F. Silva, and E. Schamiloglu, "Modeling of a Solid-State Marx Generator with Parasitic Capacitances for Optimization Studies," *Proc. 18th IEEE International Pulsed Power Conference* (Chicago, IL, 2011), p. 1422-1427.
8. M.I. Fuks and E. Schamiloglu, "Hysteresis Dependence of Mode Separation on Time-Varying Applied Voltage in a Magnetron with Diffraction Output," *Proc. 18th IEEE International Pulsed Power Conference* (Chicago, IL, 2011), p. 643-646.
9. E. Schamiloglu, "Recent Trends in High Power Microwave Source Research: Multispectral and Phase Coherent Solutions," *Proc. 2012 Asia-Pacific EMC Conference* (Singapore, May, 2012), p. 357-360.
10. N.S. Kuek, A.C. Liew, E. Schamiloglu, and J.O. Rossi, "Generating Oscillating Pulses Using Nonlinear Capacitive Transmission Lines," *Proc. 2012 IEEE Power Modulator Symposium and High Voltage Workshop* (San Diego, CA, June 3-7, 2012), p. 231-234.
11. J.O. Rossi, F.S. Yamasaki, L. Paulo da Silva Neto, and E. Schamiloglu, "Prospects of Building Capacitive Nonlinear Lines using Ceramic PZT for High-Frequency Operation," *Proc. 2012 IEEE Power Modulator Symposium and High Voltage Workshop* (San Diego, CA, June 3-7, 2012), p. 752-755.
12. A. Elfrgani, M. Fuks, S. Prasad, and E. Schamiloglu, "X-band Relativistic Backward Wave Oscillator with Two-Spiral Corrugated Bragg Reflector," *Proc. 2012 IEEE Power Modulator Symposium and High Voltage Workshop* (San Diego, CA, June 3-7, 2012), p. 756-759.
13. M.I. Fuks, E. Schamiloglu, and M.I. Petelin, "Phase Control of a Pulsed Relativistic Magnetron," *Proc. PIERS 2012* (Moscow, Russia, August 19-23, 2012), p. 726-727.
14. N.S. Kuek, A.C. Liew, E. Schamiloglu, and J.O. Rossi, "Nonlinear Inductive Line for Producing Oscillating Pulses," *Proc. 4th EuroAsian Pulsed Power Conference/BEAMS Conference* (Karlsruhe, Germany, October 1-4, 2012), p. O8A4-1-5.
15. R.L. Ives, D. Marsden, G. Collins, G. Lucovsky, D. Zeller, and E. Schamiloglu, "High Power RF Window for Multi-Megawatt Power Transmission," *Proc. IVEC 2013* (Paris, France, May 21-23, 2013), p. 978-1-4673-5977-1/13.
16. M. Liu, C. Liu, and E. Schamiloglu, "A6 Relativistic Magnetron using a Single-step Cavity with Diffraction Output," *Proc. IEEE PPS-2013* (San Francisco, CA, June 16-21, 2013), p. 6627669-1-5.
17. N.S. Kuek, A.C. Liew, E. Schamiloglu, and J.O. Rossi, "Generating RF Pulses using a Nonlinear Hybrid Line," *Proc. IEEE PPS-2013* (San Francisco, CA, June 16-21, 2013), p. 66627411-1-5.
18. J.O. Rossi, F.S. Yamasaki, N.S. Kuek, and E. Schamiloglu, "Design Considerations in Lossy Dielectric Nonlinear Transmission Lines," *Proc. IEEE PPS-2013* (San Francisco, CA, June 16-21, 2013), p. 6627410-1-4.

19. S. Prasad and E. Schamiloglu, "A Survey of Narrowband IEMI Global Threats," *Proc. IEEE International Symposium on Electromagnetic Compatibility* (Denver, CO, August 5-9, 2013), p. 397-400.
20. E. Schamiloglu, "Trends in High Power Microwaves" (Invited), *Proc. 16th Israeli Plasma Science and Applications Conference* (Tel Aviv, Israel, February 5, 2014), p. 18.
21. R.L. Ives, D. Marsden, G. Collins, G. Lucovsky, D. Zeller, and E. Schamiloglu, "Plasma Deposited Multipactor Coating for High Power, Sapphire, RF Windows," *Proc. IVEC 2014* (Monterey, CA, April 22-24, 2014), p. 185.
22. A. Elfrgani, M.I. Fuks, and E. Schamiloglu, "Power Combiner for High Power Cherenkov Devices," *Proc. IVEC 2014* (Monterey, CA, April 22-24, 2014), p. 233.

C. Presentations

1. E. Schamiloglu, "Status of Relativistic Electronics Research in Laboratories in the United States" (Invited Plenary), *Proc. 8th International Workshop on Strong Microwaves in Plasmas* (Nizhny Novgorod, Russia, 2011).
2. K.L. Cartwright, M.M. Hopkins, M.T. Bettencourt, D.A. Shiffler, W.W. Tang, K. Nichols, and E. Schamiloglu, "Verification of Emission Models for Finite Element and Finite Difference Time Domain Particle-in-Cell towards the Understanding of Variability of Field Emission Cathodes," *IEEE International Conference on Plasma Science* (Chicago, IL, June 26-30, 2011).
3. E. Schamiloglu, M. Fuks, S. Prasad, C. Leach, C. Mendonca, and D. Galbreath, "Recent Advances in Relativistic Magnetrons," *EUROEM 2012* (Toulouse, France, July 2-5, 2012).
4. E. Schamiloglu, M. Fuks, S. Prasad, C. Leach, C. Mendonca, and D. Galbreath, "Recent Advances in Relativistic A6 Magnetron Research - Improvements in Start-Up and Efficiency," *IEEE International Conference on Plasma Science* (Edinburgh, Scotland, July 9-12, 2012).
5. E. Schamiloglu, M. Fuks, S. Prasad, C. Leach, C. Mendonca, and D. Galbreath, "Recent Advances in Relativistic A6 Magnetron Research - Mode Control," *IEEE International Conference on Plasma Science* (Edinburgh, Scotland, July 9-12, 2012).
6. E. Schamiloglu, "Recent Trends in Global High Power Microwave Source Research," *Fifteenth Annual Directed Energy Annual Symposium* (Albuquerque, NM, November 26-30, 2012).
7. S. Prasad, C. Leach, C.J. Buchenauer, M. Fuks, and E. Schamiloglu, "UNM Transparent Cathode Experiments Revisited," *IEEE International Conference on Plasma Science* (San Francisco, CA, June 16-21, 2013).
8. M. Fuks and E. Schamiloglu, "Magnetron with Virtual Cathode," *IEEE International Conference on Plasma Science* (San Francisco, CA, June 16-21, 2013).
9. L. Ives, D. Marsden, G. Collins, D. Zeller, G. Lucovsky, and E. Schamiloglu, "Multipactor Coatings for Sapphire Windows using Remote Plasma Assisted Deposition," *IEEE International Conference on Plasma Science* (Washington, DC, May 25-29, 2014).
10. A. Kuskov, S. Horne, E. Schamiloglu, J. Lehr, and S. Portillo "Characterization and Analysis of a Pulse Forming Network Based 11 Stage Marx System for a High Power Microwave, Plasma and Beam Physics Test Stand," *IEEE International Conference on Plasma Science* (Washington, DC, May 25-29, 2014).
11. E. Schamiloglu, M. Liu, E. Schamiloglu, M. Fuks, B. Li, and C. Liu, "Operation Characteristics of a 12-Cavity Relativistic Magnetron with Diffraction Output when Considering Secondary and Backscattered Electrons Emission," *IEEE International Conference on Plasma Science* (Washington, DC, May 25-29, 2014).
12. M. Liu, E. Schamiloglu, M. Fuks, B. Li, and C. Liu, "Axial Leakage Current Reduction in a 12-Cavity Rising-Sun Relativistic Magnetron with a Transparent Cathode," *IEEE International Conference on Plasma Science* (Washington, DC, May 25-29, 2014).

13. S. Portillo, A. Kuskov, S. Horne, J. Lehr, and E. Schamiloglu, "Initial Characterization of a Modular Magnetically Insulated Line Oscillator Test Bed," *IEEE International Conference on Plasma Science* (Washington, DC, May 25-29, 2014).
14. E. Schamiloglu, "High Power Microwave Science," *IEEE International Conference on Plasma Science* (Washington, DC, May 25-29, 2014).
15. C. Leach, S. Prasad, M. Fuks, J. Buchenauer, J. McConaha, and E. Schamiloglu, "Experimental Verification Plan for a 70% Efficient Relativistic Magnetron with Diffraction Output (MDO)," *IEEE International Conference on Plasma Science* (Washington, DC, May 25-29, 2014).

INTERACTIONS

Professor Schamiloglu presented the following talks:

- Invited Tutorial, IVEC2011, Bangalore, India, February 21, 2011
- Invited Speaker, Middle East Technical University, Ankara, Turkey, February 24-25, 2011 (hosted by Professor Demir)
- Invited Speaker, University of Michigan's MIPSE (Michigan Institute for Plasma Science and Engineering) Seminar Series, March 16, 2011 (hosted by Mark Kushner)
- Invited Speaker, University of New Mexico Board of Regents Academic/Student Affairs & Research Committee, September 07, 2011
- Invited Speaker, INPE (Brazil's National Institute for Space Research), Sao Jose Dos Campos, Brazil, February 4, 2012 (hosted by Dr. Jose Rossi)
- Invited Speaker, Süleyman Demirel University, Isparta, Turkey, April 12, 2012 (hosted by Lutfi Oksuz)
- Invited Speaker, IEEE NPSS Local Chapter, Singapore University of Technology and Design, May 22, 2012
- Invited Speaker, AFOSR 60th Anniversary Series, July 18, 2012
- Invited Lecturer, Tsinghua University Global Scholar Lecture Series, Beijing, China, September 17-20, 2012
- Invited Lecturer, IET Seminar Lectures "Extreme Electromagnetics: The Triple Threat to Infrastructure," IET, Savoy Place, London, UK, January 14, 2013
- Invited Lecturer, Microwave Tube Research and Development Centre, Bangaluru, India, "High Power Microwaves," March 4-8, 2013
- Keynote Speaker, Raytheon Missile Systems, Tucson, Arizona, "High Power Microwave Devices and Systems," April 30, 2013
- Invited Speaker, The Albuquerque IEEE Joint Chapter, "High Power Microwave Sources, Part I: An Historical Review, Part II: Thoughts on the Future - Dispersion Engineering," May 1, 2013
- Invited Speaker, Directed Energy Directorate, SMDC, Huntsville, AL, "High Power Microwaves - The Lay of the Land," May 6, 2013
- Invited Speaker, Naval Surface Warfare Center, Dahlgren Division, VA, "Recent Advances in High Power Microwave Sources," July 24, 2013
- Invited Speaker, DARPA, Albuquerque, NM, "High Power Microwave Sources - The Lay of the Land," September 03, 2013 (DARPA scientists came to UNM to hear my presentation)
- Invited Lecturer, Weizmann Institute of Science, Rehovot, Israel, February 6, 2014 (hosted by Professor Y. Maron)
- Invited Speaker, INPE (Brazil's National Institute for Space Research), Sao Jose Dos Campos, Brazil, February 24, 2014 (hosted by Dr. Mario Ueda)
- Invited Speaker, University of Strathclyde, Glasgow, Scotland (hosted by Professor Adrian

Cross)

- Invited Speaker, MIT Plasma Science and Fusion Center, Cambridge, MA, May 16, 2014 (hosted by Professor Rick Temkin)

Professor Schamiloglu's group routinely interacts with AFRL, Calabazas Creek Research, Raytheon, and University of Michigan.

RECOGNITION

Professor Schamiloglu received the following accolades during this grant period:

- 2011: STC.UNM Creativity Award
- 2012: STC.UNM Creativity Award
- 2013: STC.UNM Creativity Award
- 2013-2015: Selected as a University of New Mexico Academic Leadership Academy Fellow
- 2013: IEEE Nuclear and Plasma Sciences Society's 2012 Richard F. Shea Distinguished Member Award
- Promoted to Distinguished Professor at the University of New Mexico (01 July 2014)

NEW DISCOVERIES, INVENTIONS, PATENTS

1. E. Schamiloglu, M.I. Fuks, H. Bosman, and S. Prasad and STC.UNM "An Eggbeater Transparent Cathode for Magnetrons and Ubitrons and Related Methods of Generating High Power Microwaves," 07893621 B2, 22 February 2011.
2. M.I. Fuks and E. Schamiloglu and STC.UNM, "Magnetron Device with Mode Converter and Related Methods," 8018159 B2, 13 September 2011.
3. 5. M.I. Fuks and E. Schamiloglu and STC.UNM, "Magnetron Having a Transparent Cathode and Related Methods of Generating High Power Microwaves," U.S. Patent 8,324,811, 12 December 2012.
4. M.I. Fuks and E. Schamiloglu and STC.UNM, "Relativistic Magnetron with no Physical Cathode," UNM Invention Disclosure, 13 June 2013.

APPENDIX A - FINAL REPORT FOR NSWC

Attached in this Appendix is the final report submitted to NSWC for the supplemental funding to Prof. Schamiloglu.



Final Report Deliverable to NSWC

**in Response to Revised SOW for FY13 BA-4 NLUAV HPM Payload,
supplemental funds to AFOSR Grant #FA9550-11-1-0200**

Title:

HPM Technology Evaluation at UNM

October 15, 2013

Technical POC:

Dr. Edl Schamiloglu

Title: Principal Investigator

Institution: University of New Mexico

Tel: 505-277-4423

Fax : 505-277-1439

e-mail: edl@ece.unm.edu

TABLE OF CONTENTS

TABLE OF CONTENTS	2
INTRODUCTION	3
METHODOLOGY	3
OVERVIEW OF ASSESSMENT	4
ASSESSMENT	8
RECOMMENDATIONS	11
MILO TESTBED	15
Rationale for Continued 6.1 Research on the UNM MILO Testbed	17
REFERENCES	20

Introduction

This final report comprises the technology assessment of high power RF sources and their ancillary technologies in support of the NLUAV development of conceptual designs and down-selection of weapon component technologies for proposed FY14-15 technology maturation.

Methodology

High power microwave (HPM) sources can be categorized in numerous ways. The most common way to characterize them is in terms of the physics of how the high power RF is generated by accelerated electrons. In this regard, HPM sources are categorized as belonging to one of three types of radiation producers [1]: i) Cerenkov radiation, ii) transition radiation, and iii) Bremsstrahlung radiation. However, for the purpose of this technology assessment, this categorization is not useful. Instead, to motivate this assessment Fig. 1 presents a plot of the weight of an HPM system (in kg) versus peak radiated power (in GW). Note that there are two trend lines identified. The black line is a trend line for single shot sources and the red line is a trend line for systems that are repetitively pulsed (10s-100s Hz). I would argue that these two trend lines bound the parameter space of interest. (This figure was prepared by E. Schamiloglu for use in a forthcoming International Electrotechnical Commission (IEC) publication [2]. Although the figure was developed for land-mobile and land-transportable HPM systems, it has relevance to UAVs as well.) This is representative data relevant for sample land-mobile or land-transportable systems and includes the weight of the entire HPM system, from prime power to antenna. This was generated by combining data from Table 2.1 in [3] for the HPM sources, and models from HEIMDALL for the weight of HPM system components [4]. This figure highlights the reality that there is a broad parameter trade space for HPM sources where pulsewidth, repetition rate, bandwidth, peak power, *etc.*, all have to be balanced with the significant requirement of volume and mass.

Figure 2 presents a map of parameter space in power/frequency occupied by sophisticated HPM sources, and Fig. 3 presents peak power and energy from continuous and pulsed (durations shown) microwave sources, both narrowband and wideband. These are additional considerations that will assist with the organization of the technology assessment.

The reason why the physics of HPM production is not a useful metric to organize this technology assessment is further evident from Fig. 4, which is a schematic of the 2 MW cw gyrotron being developed for use on ITER. The volume of the beam/wave interaction space where HPM is produced is less than 1% of the entire volume of the device. This small space is the most important part of it from a physics consideration. However, from a practical consideration, the entire system is required in order for the HPM source to operate! Therefore, the entire system needs to be considered when designing an HPM source for deployment on a mobile platform.

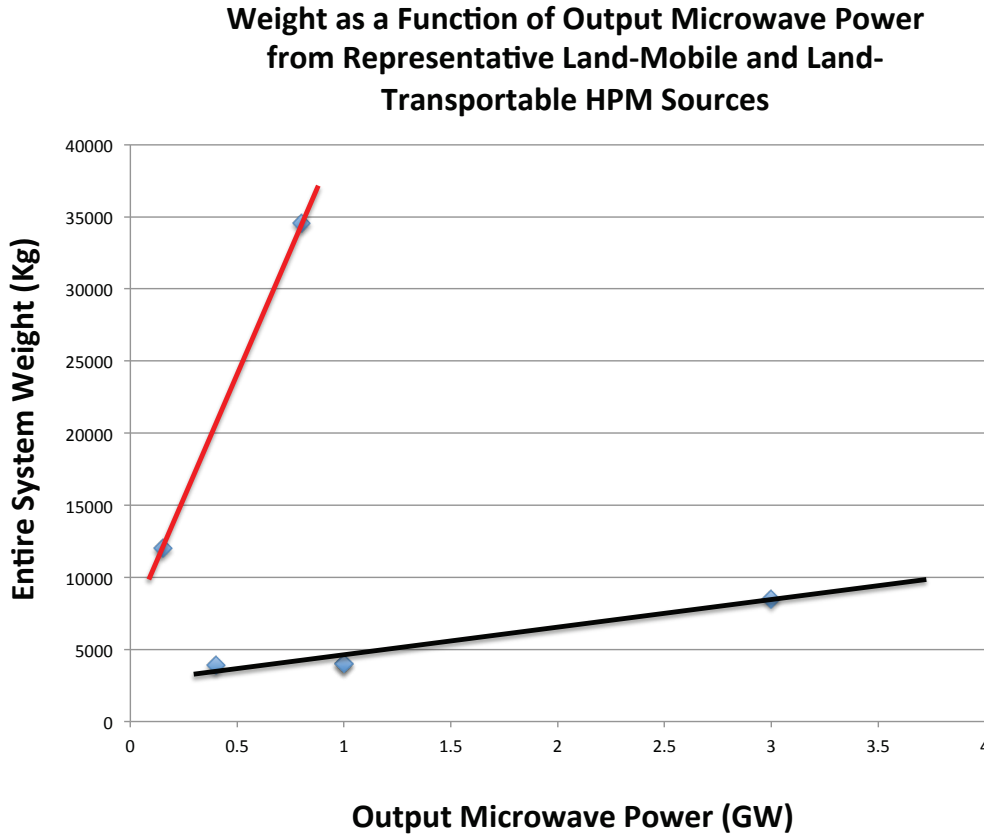


Figure 1. Plot of entire HPM system weight as a function of output microwave power for land-mobile and land-transportable systems. The black line is a trend line for single shot sources and the red line is a trend line for systems that are repetitively pulsed (10s-100s Hz).

Overview of Assessment

Now that we have determined that a physics-based HPM source categorization/assessment is not useful, let us put forth our approach for developing this assessment. Given the volume and mass constraints on the mobile platforms of interest, it is of upmost interest to identify HPM sources with the highest overall system (“wall-plug”) efficiency, not highest electronic efficiency.

Moving forward, Fig. 5 presents our motivating figure for completing this assessment. Our assumption is that the frequency range of interest is fixed, say <1 GHz to about 10 GHz. At this point we will not concern ourselves with frequency agility or frequency bandwidth, although we will address this in the final report.

In the context of the parameters that we have identified and the boundaries we have imposed, we postulate a hierarchy of sources of interest based on efficiency and effectiveness. The assumption is that an electrical applied magnetic field is a big deal. In

other words, sources that do not require an electro-magnet to generate a magnetic field simply win. They win in terms of highest system efficiency [3], a prime consideration when packaging an HPM source in a compact, mobile platform. With this in mind we outline below our assessment (in no particular order).

Class 1: Sources requiring no electro-magnet

- Reltron
- Vircator
- Relativistic magnetron with permanent magnet magnetic field
- MILO
- Linear Cerenkov source with permanent magnet magnetic field

Class 2: Sources requiring electro-magnet

- Relativistic magnetron with electro-magnet
- Linear Cerenkov sources with electro-magnet
- Klystrons – with electro-magnet
- Other remaining source configurations (gyrotrons and other free electron masers, among other source types) – with superconducting magnet

Class 3: Beamless Sources

- Ultra-wideband sources
- Nonlinear transmission line-based sources

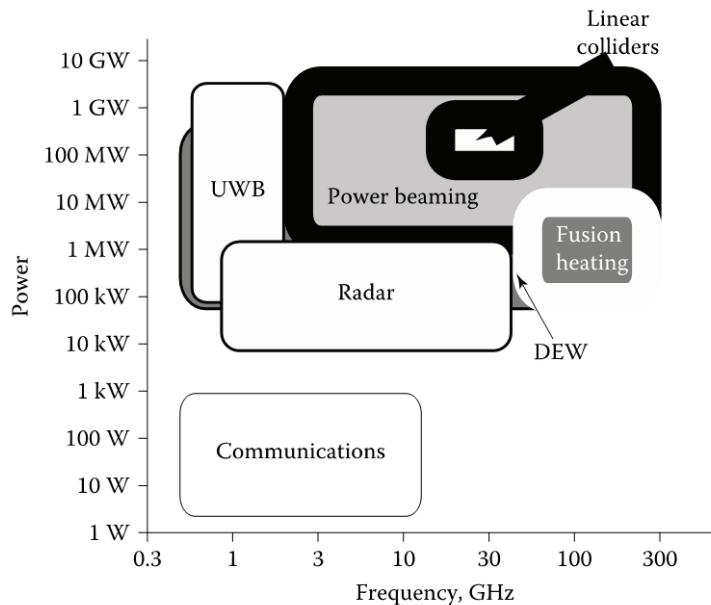


Figure 2. Parameter space in power/frequency occupied by sophisticated HPM sources (DEWs, black shaded region) [5].

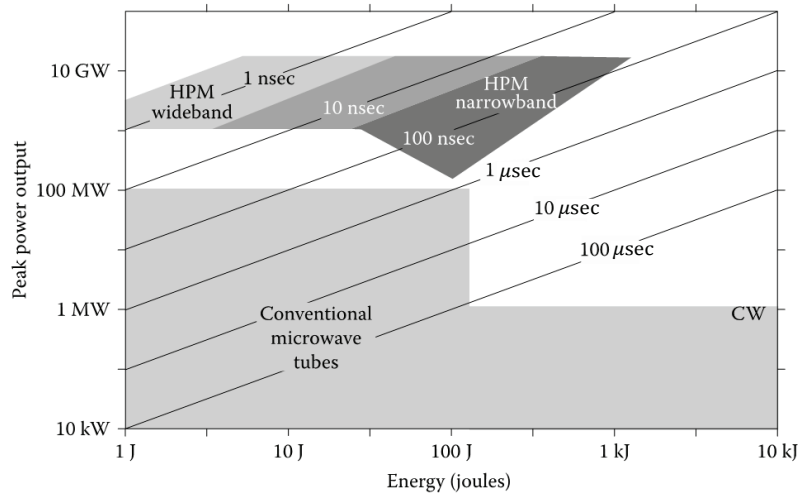


Figure 3. Peak power and energy from continuous and pulsed (durations shown) microwave sources, narrowband and wideband [5, with corrections]. Note the extremely small energy content in wideband HPM.

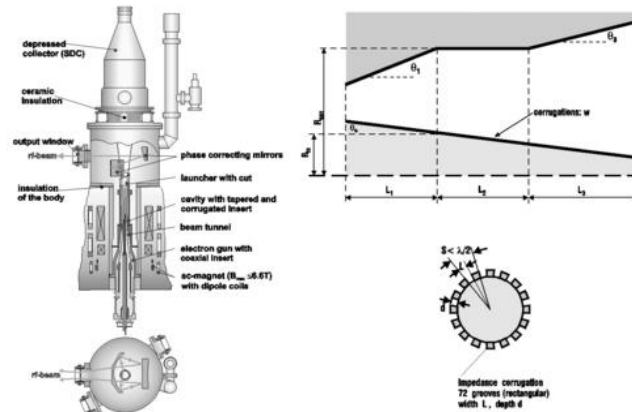


Figure 4. Schematic of the 2 MW cw gyrotron developed for ITER. The actual region where the HPM is produced takes less than 1% of the volume of the entire gyrotron.

As mentioned earlier, the volume of the HPM source (RF interaction region) by itself is a small fraction of the volume of an actual HPM system. The pulsed power driver is larger by far. Therefore, the pulsed power driver needs to be considered as the critical component of the overall system [6]. Power supplies have not been mentioned much thus far. Yet, as we pointed out, the HPM tube is typically a small fraction of the size and weight of an HPM weapon system design. The bulk of the device lies in its power-generating and conditioning equipment [7]. In 1988, Florig [7] gave a rough power supply size scaling for two classes of sources. For the 0.5 to 2 MJ/pulse class, he estimated the volume at 3 to 10 cubic meters. For the 5 to 20 MJ/pulse class, he estimated the volume at 30 to 100 cubic meters. Although he was discussing Star Wars class sources which have never been built, and although the largest reported single pulse

energy of the sources discussed above is on the order of 1 kJ, or 0.001 MJ/pulse, it would not be reasonable to reduce his 3 cubic meters by a factor of 500 to get 0.006 cubic meters (0.22 cu ft.). The actual power supply that drove the 1 kJ RKA was much larger. Much higher energy densities can be achieved in explosive sources, but they are limited and not part of this assessment.

Nevertheless, progress has been made since 1988 and, although unpublished, it is safe to assume that the power densities available today are measurably larger than what Florig reported in 1988.

In 2004 Schamiloglu *et al.* described pulsed power drivers in the context of the “mouse-to-elephant” curve in biology [8]. This is reproduced in Fig. 5. The point of this is that, in biology what mammals have in common is that they all breathe oxygen and are carbon-based life forms. That is why there is this relationship between metabolic rate and body size. In pulsed power, common materials are used in all pulsed power accelerators so that it makes sense that there should be a similar relationship between power and size.

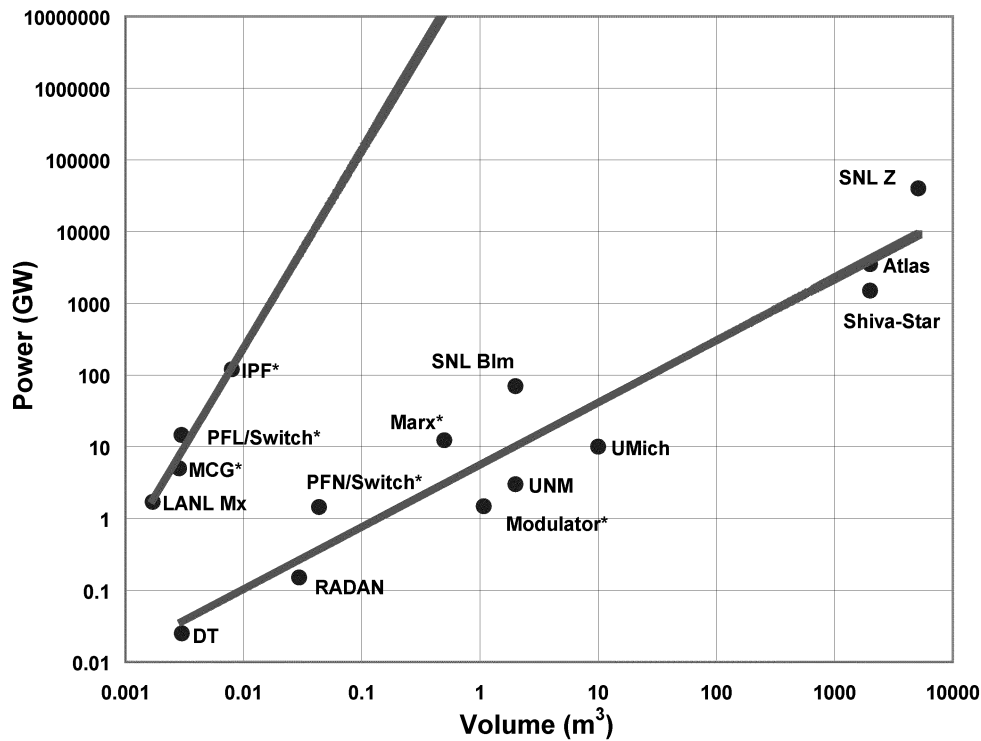


Figure 5. The analogy of the mouse-to-elephant curve in pulsed power. The line with the faster rising slope comprises systems either driven by explosives or that use state-of-the-art high energy density components. The line with the lower slope represents more traditional pulsed power systems found in the laboratory.

Assessment

This final report presents the assessment of this technology. In order to address the requirements, we must identify the limitations imposed by the payload and the application. The numbers that I am using are best estimates and may not reflect the actual limitations, but are surely in the ballpark.

Payload limitation – our constraint

- Weight \leq 1000 kg
- Diameter \leq 0.75 m
- Length \leq 2.5 m

Rep-rate limitation – modeling

The fundamental limitation to rep-rate in HPM sources of relevance to this assessment is outgassing from components within the pulsed power-driven electron beam source. All such sources use explosive electron emission (EEE) cathodes that operate in the space-charge-limited regime. This is, by far, the most significant source of outgassing in the HPM source. Velvet is the most popular cathode material since it “turns-on” at 30 kV/cm and produces current densities in excess of 1 kA/cm² [9]. Therefore, we will be using velvet cathode material as the basis for modeling the outgassing and, therefore, the rep-rate limitation in HPM sources. (It should be noted that Shiffler *et al.* [10] have demonstrated that CsI-coated carbon fiber cathodes emit much less gas than velvet cathodes. However, in this assessment we will use the modeling results for velvet since this cathode material is more prevalent and the conclusions drawn will be more conservative.)

Through diverse mechanisms, the application of a strong electric field results in plasma formation on the cathode surface. The electric field then extracts a space-charge-limited electron flow from this plasma. The ensuing expansion of the cathode plasma into the anode-cathode (*A-K*) gap reduces the diode impedance, and can ultimately result in diode shorting of the high-voltage pulse.

Several materials have been used as cold cathode explosive emitters in a variety of cathode configurations. As mentioned earlier, one of the most successful of these is the cloth fiber – velvet cathode. This material has a low electric field threshold for plasma initiation, emits very uniformly, and has low gap closure velocities. It is also inexpensive and easy to use. However, it is unsuitable for some repetitive pulse applications because it discharges a significant amount of matter during a pulse, and its lifetime is limited to tens of thousands of pulses because of erosion of the velvet fibers.

Work by Miller [9] has determined that explosive emission from velvet is initiated by a surface flashover mechanism. The surface discharge gives rise to a cold dense plasma/gas column. A phenomenological model based on resistive heating of the plasma columns

appears to give a good estimate for the final diode-plasma closure velocity. Guided by these results, we have explored the rep-rate limitation in HPM sources utilizing explosive emission cathodes, with velvet being the worst-case scenario.

Velvet cathode material discharges a significant amount of matter during the EEE process. Early in time this matter predominantly comprises surface contaminants, e.g., water vapor and vacuum pump oils that are desorbed from the large surface area of the dense fiber array, in addition to some eroded velvet fiber. At later times in the lifetime of the cathode, fiber erosion becomes increasingly important. The term “conditioning” is often used to describe an initial period (perhaps covering several hundred shots) in which adsorbed material is discharged from the velvet.

We can crudely estimate the equilibrium pressure in the HPM source vacuum region under repetitive pulse conditions using the following argument [9]. Let N_p be the number of molecules liberated from the cathode during a pulse, R is the repetition rate, and S_{eff} is the effective pumping speed of the vacuum system. If the base pressure is sufficiently low, then the equilibrium pressure is approximately given by

$$P(\text{Torr}) = \frac{N_p (\text{atoms/pulse}) R (\text{pulses/s})}{[3.5 \times 10^{19} \text{ atoms/l/Torr}] S_{\text{eff}} (\text{l/s})}. \quad (1)$$

A typical vacuum pump used on such a system would be a turbomolecular pump with pumping speed $S = 300 \text{ l/s}$. The effective pumping speed S_{eff} of the vacuum system depends on the system conductance C according to

$$S_{\text{eff}}^{-1} = S^{-1} + C^{-1}. \quad (2)$$

A useful approximation for the vacuum conductance of a cylindrical tube of diameter D and length L is given by (with dimensions in cm)

$$C (\text{l/s}) = 12.1 \frac{D^3}{L}. \quad (3)$$

For an S-band HPM source (S-band since the UNM MILO is this size), the beam pipe diameter is roughly 5 cm, increasing to about 15 cm for an L-band source. The distance from the cathode to the vacuum is estimated to be 50 cm. Therefore, $(S_{\text{eff}})_{\text{L-band}} = 175 \text{ l/s}$, but $(S_{\text{eff}})_{\text{S-band}} = 15 \text{ l/s}$. Solving Eq. (1) for N_p , assuming $P = 10^{-4} \text{ Torr}$ and $R = 1 \text{ Hz}$ for the L-band source and $R = 0.5 \text{ Hz}$ for the S-band source yields $(N_p)_{\text{L-band}} = 6.2 \times 10^{17} \text{ mole/pulse}$ and $(N_p)_{\text{S-band}} = 1.0 \times 10^{17} \text{ mole/pulse}$. For a linear source such as a Reltron the area of the cathode for an L-band source would be about 180 cm^2 , while for an S-band source it is about 28 cm^2 . Therefore, it appears that after an initial conditioning period, velvet discharges approximately $N_A = 3.5 \times 10^{15} \text{ mole/cm}^2$ per

pulse. The area of the cathode in a MILO can be much larger. For the S-band MILO at UNM, the cathode area is approximately 100 cm^2 , about four times the area of a Reltron S-band cathode.

Miller points out that if an HPM source is operated at 1 Hz repetition rate at a pressure a few times 10^{-4} Torr then microwaves will cease to be generated, the voltage pulse will be degraded, and the velvet will be severely damaged [9]. This is attributed to the generation of ions in the *A-K* gap through an avalanche process with subsequent ion backbombardment of the cathode, and the liberation of additional matter from the cathode surface. A useful estimate for this condition in hydrogen is given by [11]

$$\tau_i (\text{ns}) = \frac{0.33}{P(\text{Torr})}. \quad (4)$$

Substituting this into Eq. (1) yields a limiting expression for the pulse repetition rate

$$R(\text{Hz}) < \frac{3300 S_{\text{eff}} (l/s)}{A_c (\text{cm}^2) \tau (\text{ns})}, \quad (5)$$

where A_c is the cathode area. For a $1 \mu\text{s}$ pulse length, a cathode of 30 cm^2 , and an effective pumping speed of 100 l/s , the repetition rate is limited to about 10 Hz.

Miller performs a careful assessment of the dynamics of the liberation of matter from velvet cathodes as a function of tuft dimensions and packing density [9]. A good scaling relationship for plasma closure velocity was determined to be

$$v_f (\text{m/s}) = 100 \left(\frac{d^*}{d} \right)^{2/3} V^{1/2} \quad (6)$$

for diode voltage V , tuft separation d^* , and *A-K* gap d . Equation (6) suggests that the closure velocity varies as the cube root of the diode current density. Assuming that the useful pulse duration is limited by an increase in the diode perveance of 20%, then Eq. (6) leads to a limitation of the diode voltage pulse that can be approximated as

$$\tau (\text{s}) < 0.001 d^{5/3} (d^*)^{-2/3} V^{-1/2} \quad (7)$$

with physical dimensions in meters and V in volts.

A second limitation on pulse duration can be obtained by modifying Eq. (5) to include tuft densities different from the standard “red” velvet, according to

$$\tau (\text{ns}) < \left(\frac{3300 S}{A_c R} \right) \left(\frac{d^*}{0.07} \right)^2 \quad (8)$$

with d^* now in cm. Increasing the tuft spacing reduces the amount of material vaporized in a pulse, resulting in longer useful pulse duration for a given vacuum system and repetition rate. However, the increased tuft spacing can also limit the useful pulse duration by increasing the plasma closure velocity.

Recommendations

Due to the constraints of the payload, we eliminate from consideration the Class 2 and Class 3 sources listed earlier. The Class 2 sources require an electrical magnet and therefore simply cannot be considered from a system efficiency standpoint. The Class 3 sources are eliminated because the NLTL sources represent an immature technology that has yet to achieve reliable operation at the frequencies and power levels of interest. They also have a large volume requirement that is unsuitable for the payload under consideration. They also require constant maintenance and adjustment to synchronize the multiple NLTL lines used to drive one antenna array.

The wideband sources or impulse-type sources might be of interest for a limited target set. However, for the constraints of the payload, it is unlikely that they have the energy content in the RF field that is of use in the application under consideration.

This leaves the Class 1 sources:

- Reltron
- Vircator
- Relativistic magnetron with permanent magnet magnetic field
- MILO
- Linear Cerenkov source with permanent magnet magnetic field

From the Class 1 sources we eliminate the linear Cerenkov source with permanent magnetic field since permanent magnets are infeasible for an L- or S-band Cerenkov source. (It should be noted that linear Cerenkov sources require magnetic fields of about 3 T, whereas relativistic magnetrons require less than half that amplitude.) A permanent magnet solution is possible at X-band, but this frequency range is not of interest for the application.

From the Class 1 sources we also eliminate the Vircator for two reasons. First, the Vircator has a very low efficiency, single digit. That is an issue for the payload energy/power constraints. Secondly, a Vircator typically requires grids (screen mesh) and it is difficult to consider how the device with grids can be hardened to survive the g-forces on the payload.

From the Class 1 source we also eliminate the Reltron for three reasons. The Reltron is similar to klystrons in that microwave power is extracted from a bunched beam using a set of output cavities; however, it is unique in two respects. First, the bunching

mechanism differs from that in a klystron, and, second, the bunched beam is reaccelerated to higher energy to increase the energy withdrawn in the output cavities. The cavities used in the Reltron are rather large in diameter, particularly in L-band, but also in S-band. They will not be able to fit within the constraints of the payload. Second, the Reltron, by necessity, is a rather long device because of the extraction cavity and the interaction of the beam bunches. It will not be possible to accommodate the pulsed power and the Reltron within the payload. Third, the Reltron also uses grids in the cavities and hardening them to g-forces is a tremendous challenge.

Figure 6 summarizes these conclusions in terms of efficiency regarding the use of Class 1 and Class 2 sources in the payload and application under consideration and Fig. 7 summarizes these conclusions in terms of system mass/volume.

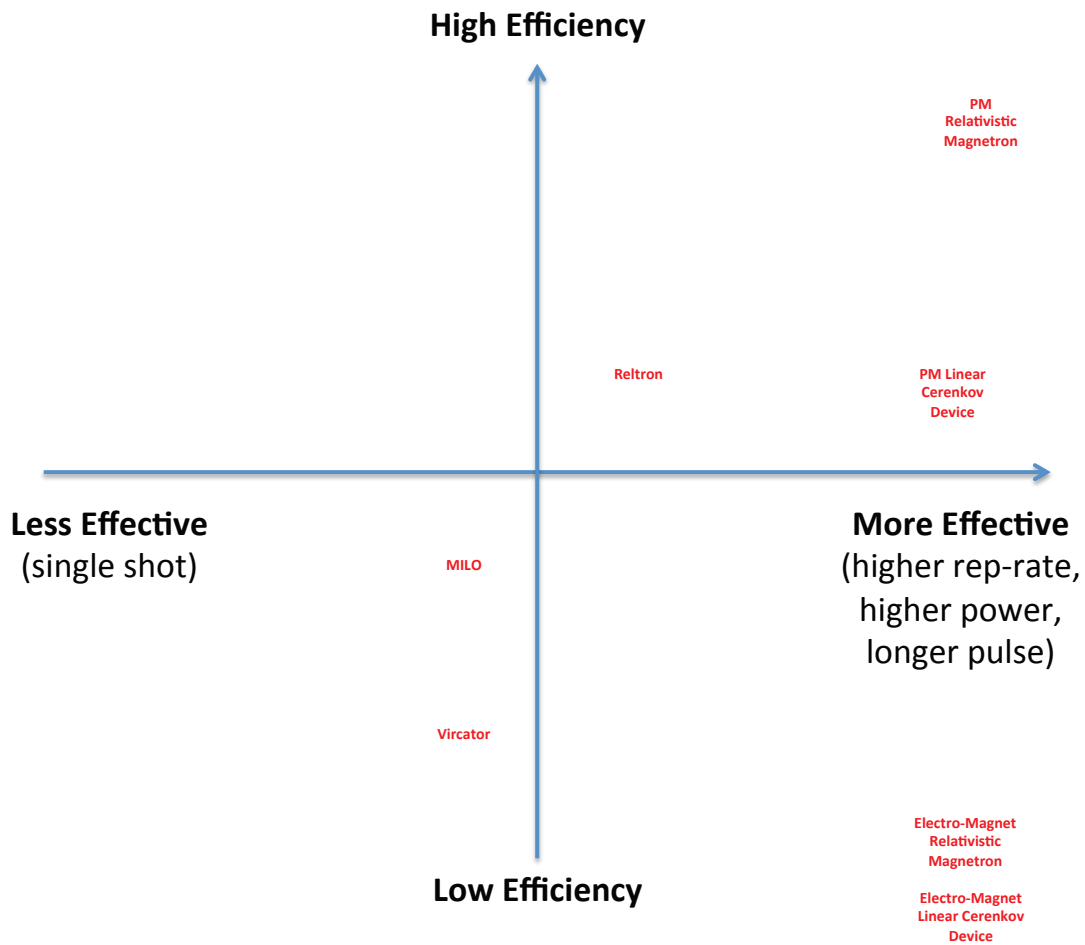


Figure 6. Parameter space to be identified in this assessment in terms of total efficiency. The desirable sources would lay in the first quadrant (top right), assuming that the frequencies of interest are about the same. PM=permanent magnet.

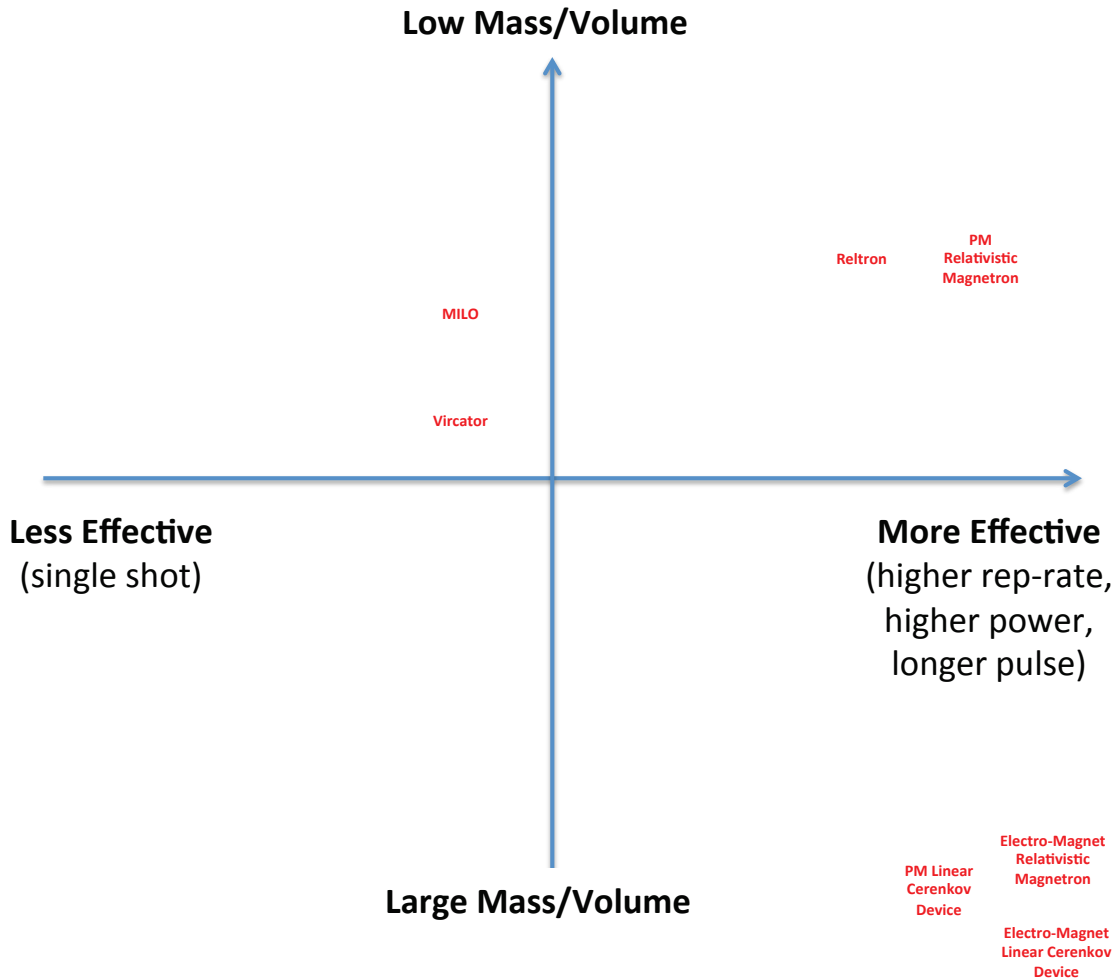


Figure 7. Parameter space to be identified in this assessment in terms of total mass/volume. The desirable sources would lay in the first quadrant (top right), assuming that the frequencies of interest are about the same. PM=permanent magnet.

From Figs. 6 and 7 it is pronouncedly clear that the permanent magnet relativistic magnetron is the only viable solution for the payload and application under consideration. This is not surprising. The relativistic magnetron (the HPM source by itself, not including any other component of the system) is the most compact of any HPM source. In addition, it is the HPM source with the highest beam-to-microwave conversion efficiency, as was demonstrated in [12]. The reason for these two observations is that, unlike other HPM sources, in the relativistic magnetron the electron source (the cathode, or electron gun) sits within the electromagnetic interaction region. Thus, the cathode and the electromagnetic interaction region occupy the same volume, unlike linear beam devices where the cathode is external to the electromagnetic interaction region. Also, the high efficiency is a result of the fact that electrons are recirculant in the relativistic magnetron, whereas in linear beam devices the electrons perform a single pass through the system before hitting the beam dump. This is illustrated in Fig. 8.

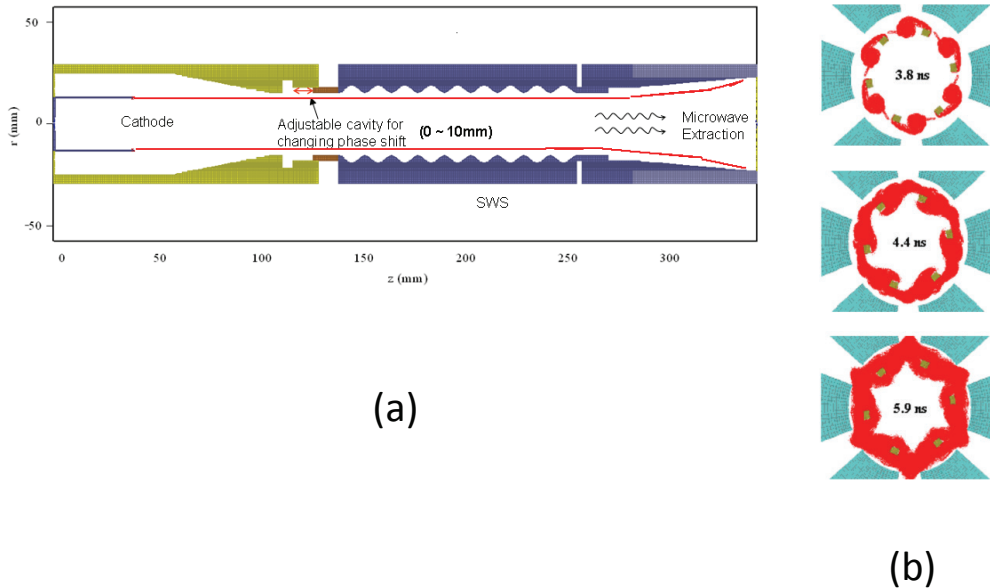


Figure 8. (a) Electrons in a linear-beam are injected from outside the electromagnetic interaction region (shown as a particle-in-cell (PIC) simulation of a backward-wave oscillator at the University of New Mexico) and perform a single pass through the system. (b) Electrons in a relativistic magnetron (shown as a PIC simulation of the A6 relativistic magnetron driven by a transparent cathode at the University of New Mexico) are recirculant, thereby leading to much higher beam-to-microwave conversion efficiency.

Payload limitation – our constraint

- Weight \leq 1000 kg
- Diameter \leq 0.75 m
- Length \leq 2.5 m

A custom, compact pulsed power driver using batteries as primary energy can be designed to readily fit in the payload constraint. Matched to a relativistic magnetron with radial extraction, one can envision a complete system being fitted into a representative pod, similar to one shown in Fig. 9. Permanent magnets are used to provide the axial magnetic field in the device and they weigh about 250 lbs for an S-band source [13]. Output power levels up to 1 GW are feasible. Pulse repetition rate and pulse length are constrained by the pulsed power driver. I anticipate that 10 Hz repetition for a burst lasting a few minutes for 50 ns-length pulses is feasible. Driving voltages would be around 350 kV and the impedance of the relativistic magnetron would be about 40 Ω . A permanently sealed variant of the device would mitigate the need for vacuum hardware.

This is the only solution currently deemed viable for the proposed payload and application. However, the MILO might also represent a viable solution, provided that some 6.1 research investment is made. This is described next.

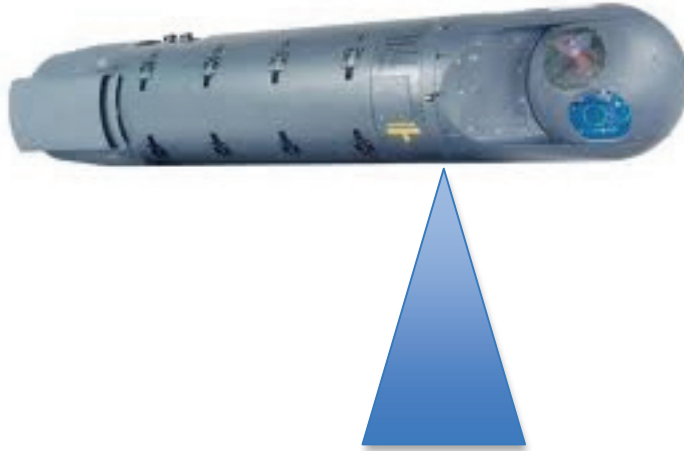


Figure 9. A representative pod that can contain the entire relativistic magnetron system (image from aviationnews.eu). The blue represents the output from the radial extraction through a conformal radome maintaining sealed vacuum within the device.

MILO Testbed

The reason why the relativistic magnetron won over the MILO is that the operating efficiency of the relativistic magnetron can be high, 50-70%, depending on the extraction technique. The efficiency of the MILO is about 20% at best, with certain variants achieving 25%. The fundamental reason for this is that the MILO relies on a self-magnetic field due to the axial electron flow to magnetically insulate the device.¹ The head of the electron flow is “wasted,” lost to the vanes because the self-magnetic field has yet to be formed. This is the inherent reason for the low efficiency, part of the electron flow is used to generate self-magnetic insulation and does not contribute to microwave generation.

However, the fact that the MILO does not require an external permanent magnet makes it worthwhile to pursue its development for future applications. A MILO-based system might be lighter than a permanent magnet relativistic magnetron-based system.

Another issue with the MILO is the large cathode area involved. This leads to a lot of gas build-up and limits the repetition rate and microwave pulse length. However, through research this can also be improved upon.

Figure 10 presents a cutaway drawing of the UNM MILO Testbed. Its construction was sponsored through NSWC, and is shown in Fig. 11.

¹ The MILO is very similar to a relativistic magnetron. The key difference is that the interacting electron flow is in the axial direction, as in a linear beam device. The physics of microwave generation is a hybrid interaction between a magnetron and a Cerenkov device.

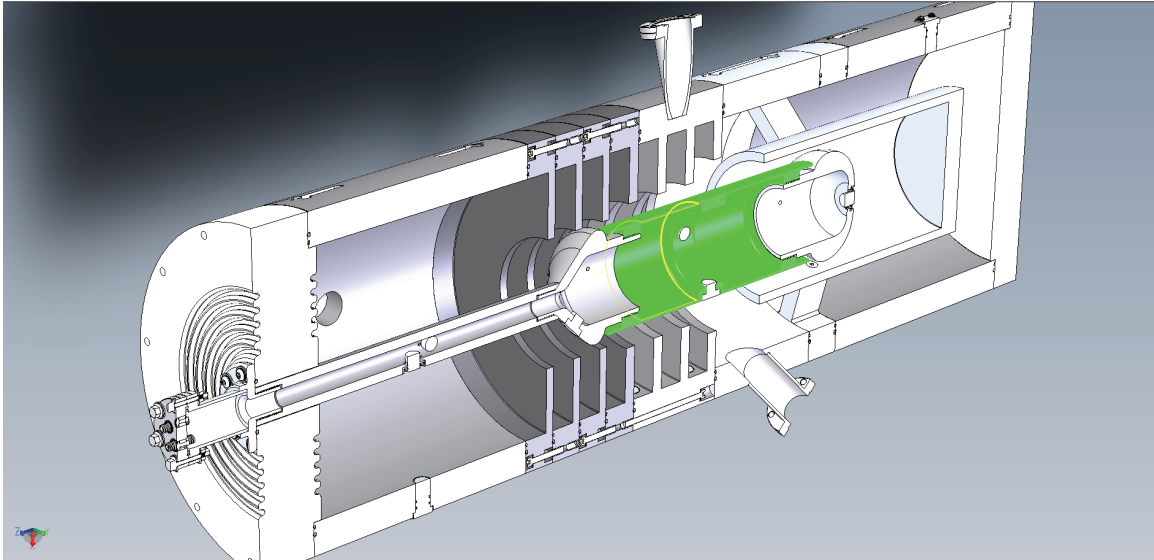


Figure 10. Cutaway drawing of the UNM MILO Testbed. The green represents the cathode.

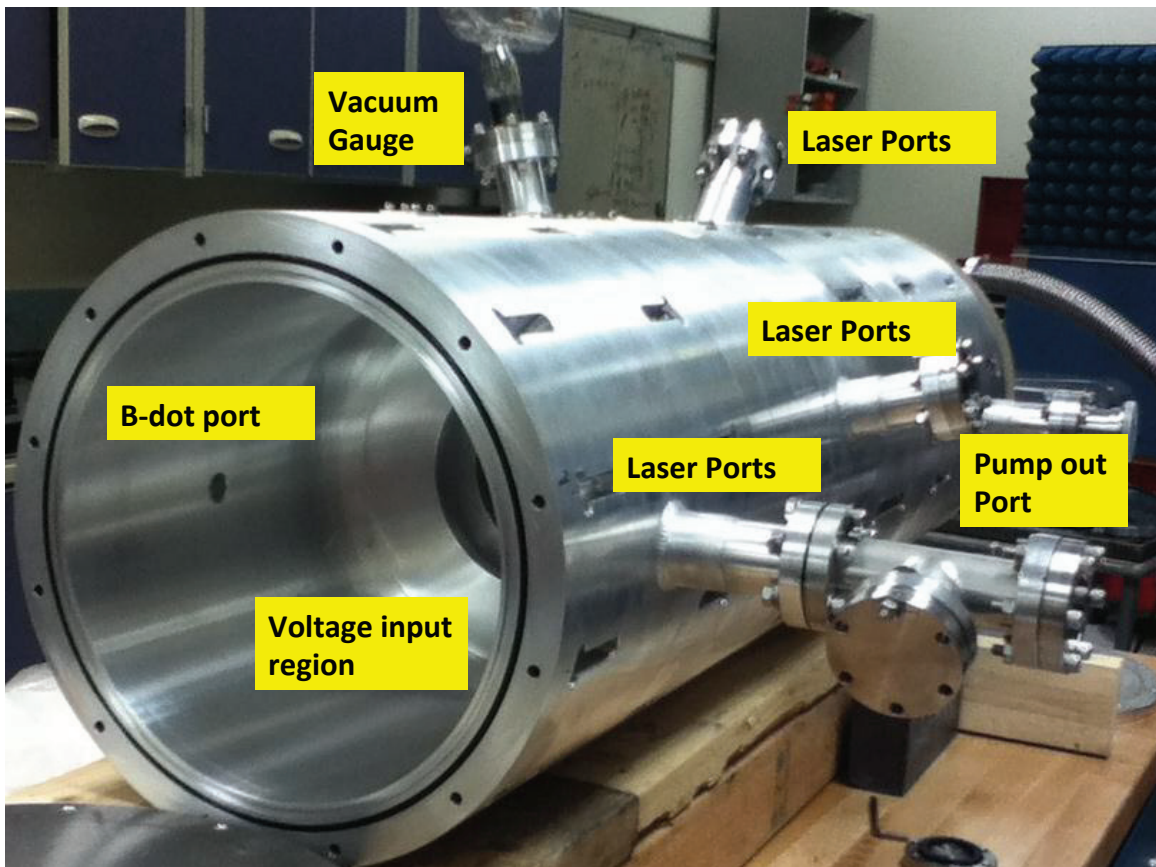


Figure 11. Photograph of the constructed UNM MILO Testbed.

Figure 12 presents a photograph of the UNM MILO Testbed under vacuum.

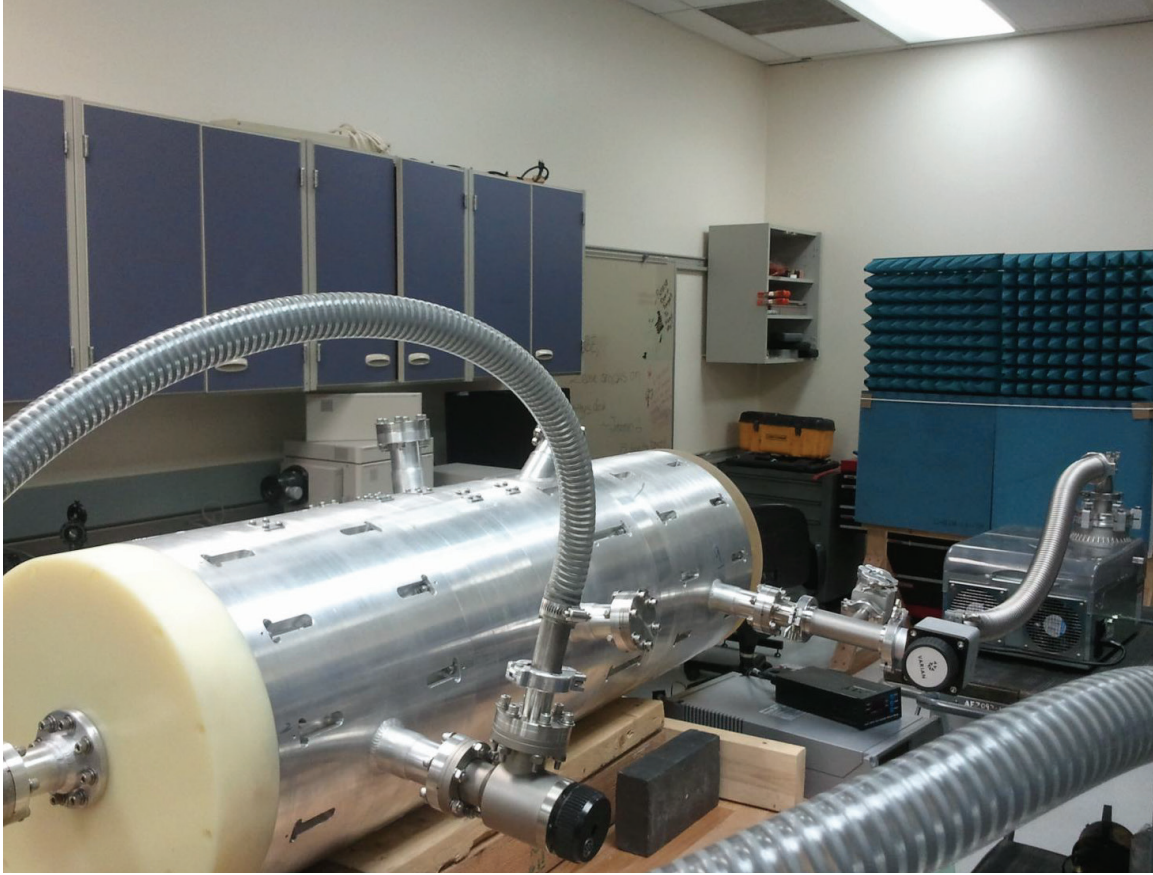


Figure 12. Photograph of the UNM MILO Testbed under vacuum.

Rationale for Continued 6.1 Research on the UNM MILO Testbed

Microwave pulse shortening in long pulse beam-driven sources, low efficiency, as well as poor repetition rate has long posed a problem for HPM sources and limited their use for DoD applications. UNM is proposing a basic (6.1) research program to investigate gap closure physics problems in beam driven devices in order to develop and transition to DoD high power long pulse >500 ns HPM sources with high efficiency and high repetition rate. We propose:

- To investigate the plasma closure mechanism leading to pulse shortening in magnetically insulated HPM devices such as relativistic magnetrons and MILOs.
 - Models point to low density plasmas evolving from the cathode surface as main driver of radiation collapse. Plasma diagnostics can be used to observe spatial and temporal evolution of such plasmas in the MILO Testbed.
- Develop materials and techniques to mitigate this plasma closure and increase the pulse length in excess of 500 ns.
 - Carbon nanotube cathodes, transparent cathodes.

- Understand and solve the ion production and gap closure problem to yield solutions for repetitive pulsing of beam driven HPM sources. Experimental results can be compared with the modeling results proposed earlier.
- Develop a more thorough understanding of the beam physics in magnetically insulated devices to fundamentally increase the energy transfer efficiency.

Figure 13 and 14 present some recent simulation results using the Voss Scientific/ATK Mission Research LSP code [14]. This ability to introduce plasmas (electrons and ions) in a PIC simulation is a recent development and represents a powerful tool to use to study increasing MILO efficiency.

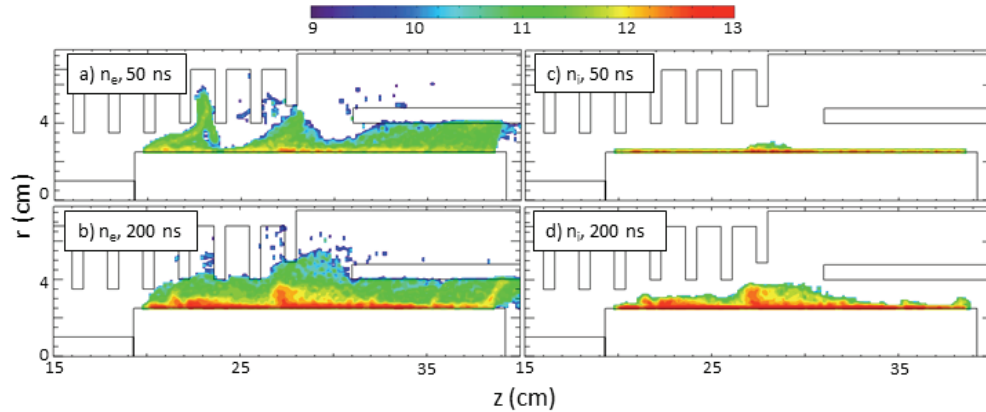


Figure 13. PIC numerical models of electron and cathode plasma densities at 50 and 200 ns. Initially the cathode plasmas are relatively close to the cathode and radiated power is maintained. At 200 ns, the cathode plasmas are clearly deep in the interaction space and are mixing with the electron sheath and the radiation output disappears.

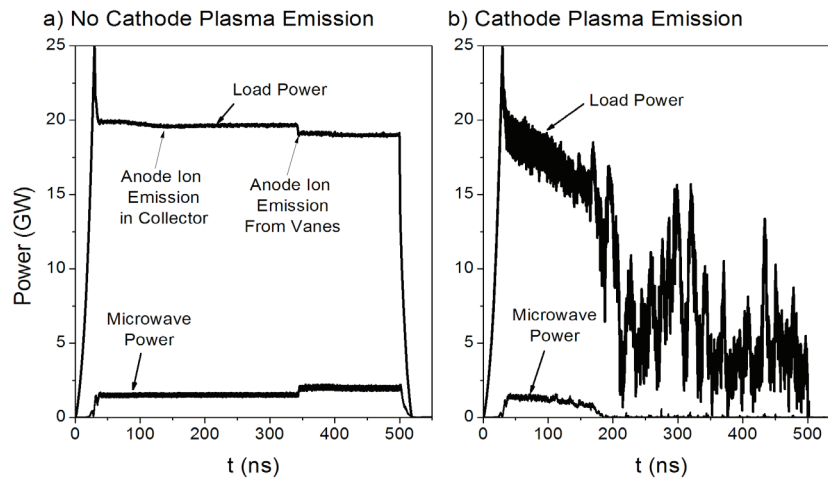


Figure 14. Numerical simulation of MILO output power with no cathode plasmas and with cathode plasma emission. Plasma emission rate is set to 100 A/cm². Impedance collapse has occurred around the 200 ns mark where models show plasma density deep into the interaction space.

A robust 6.1 program that combines the use of LSP PIC simulations with ions and electrons and utilizes the UNM MILO Testbed can make an important contribution to the feasibility of employing the MILO in future payloads of interest to the DoD.

References

1. S.H. Gold and G.S. Nusinovich, “Review of High-Power Microwave Source,” *Rev. Sci. Instrum.*, vol. 68, 3945 (1997).
2. A. Wraight *et al.*, “IEMI Immunity Test Methods for Equipment and Systems,” IEC Project Number 61000-4-36 Ed 1.0, IEC Document Number 77C/222/CD (in preparation, 2013).
3. R.J. Barker and E. Schamiloglu, *High Power Microwave Sources and Technologies* (IEEE Press/John Wiley and Sons, New York, NY, 2001).
4. J.A. Swegle and J.N. Benford, “End-to-End Modeling with the Heimdall Code to Scope High-Power Microwave Systems,” *Proc. 2007 IEEE International Pulsed Power Conference, PPPS-2007* (Albuquerque, NM, June 2007), pp. 1114-1118.
5. J. Benford, J. Swegle, and E. Schamiloglu, *High Power Microwaves, 2nd Ed.* (Taylor and Francis, Boca Raton, FL, 2007).
6. L.D. Bacon and L.F. Rinehart, “A Brief Technology Survey of High-Power Microwave Sources,” Sandia National Laboratories Report SAND2001-1155 (Sandia National Laboratories, Albuquerque, NM, April 2001).
7. H. Florig, The Future Battlefield: A Blast of Gigawatts,” *IEEE Spectrum*, vol. 25 (1988), pp. 50-54.
8. E. Schamiloglu, R.J. Barker, M. Gundersen, and A.A. Neuber, “Modern Pulsed Power: Charlie Martin and Beyond,” in *Proceedings IEEE*, vol. 92 (2004), pp. 1014-1020.
9. R.B. Miller, “Mechanism of Explosive Electron Emission for Dielectric Fiber (Velvet) Cathodes,” *J Appl. Phys.*, vol. 84, 3880 (1998).
10. D. Shiffler, M. LaCour, K. Golby, M. Sena, M. Mitchell, M. Haworth, K. Hendricks, and T. Spencer, “Comparison of Velvet and Cesium Iodide-Coated Carbon Fiber Cathodes,” *IEEE Trans. Plasma Sci.*, vol. 29, 445 (2001).
11. C.L. Olson, *Phys. Rev. A.*, vol. 11, 288 (1975).
12. M.I. Fuks and E. Schamiloglu, “70% Efficient Relativistic Magnetron with Axial Extraction of Radiation Through a Horn Antenna,” *IEEE Trans. Plasma Sci.*, vol. 38, 1302 (2010).
13. Andrey Andreev (Raytheon/Ktech, private communication, 2013).
14. D.V. Rose *et al.* (under review, 2013).